ISTANBUL TECHNICAL UNIVERSITY ★ GRADUATE SCHOOL

FABRICATION OF MULTI-COMPONENT SUPERPARAMAGNETIC NANOPARTICLES AND MAGNETIC HEATING PERFORMANCE FOR HYPERTHERMIA CANCER THERAPY

M.Sc. THESIS

Ayşesimay ÇETİN

Department of Nanoscience and Nanoengineering

Nanoscience and Nanoengineering Programme

FEBRUARY 2021

ISTANBUL TECHNICAL UNIVERSITY ★ GRADUATE SCHOOL

FABRICATION OF MULTI-COMPONENT SUPERPARAMAGNETIC NANOPARTICLES AND MAGNETIC HEATING PERFORMANCE FOR HYPERTHERMIA CANCER THERAPY

M.Sc. THESIS

Ayşesimay ÇETİN
(513171012)

Department of Nanoscience and Nanoengineering

Nanoscience and Nanoengineering Programme

Thesis Advisor: Assoc. Prof. Dr. Ali KILIÇ

FEBRUARY 2021

ISTANBUL TEKNİK ÜNİVERSİTESİ ★ LİSANSÜSTÜ EĞİTİM ENSTİTÜSÜ

HİPERTERMİ KANSER TERAPİSİ İÇİN ÇOK BİLEŞENLİ SÜPERPARAMANYETİK NANOPARTİKÜLLERİN ÜRETİMİ VE MANYETİK ISINMA PERFORMANSI

YÜKSEK LİSANS TEZİ

Ayşesimay ÇETİN
(513171012)

Nanobilim ve Nanomühendislik Anabilim Dalı

Nanobilim ve Nanomühendislik Programı

Tez Danışmanı: Doç. Dr. Ali KILIÇ

ŞUBAT 2021

Ayşesimay Çetin, a M.Sc. student of İTU Graduate School student ID 513171012, successfully defended the thesis entitled "FABRICATION OF MULTI-COMPONENT SUPERPARAMAGNETIC NANOPARTICLES AND MAGNETIC HEATING PERFORMANCE FOR HYPERTHERMIA CANCER THERAPY", which she prepared after fulfilling the requirements specified in the associated legislations, before the jury whose signatures are below.

Thesis Advisor :	**Assoc. Prof. Dr. Ali KILIÇ** Istanbul Technical University	.....
Jury Members :	**Prof. Dr. Ali DEMİR** Istanbul Technical University	.....
	Assist. Prof. Dr. Çiğdem TAŞDELEN YÜCEDAĞ Gebze Technical University	.....

Date of Submission : 22 January 2021
Date of Defense : 16 February 2021

To my family,

FOREWORD

First of all, I would like to thank to Prof. Dr. Celaletdin Ergun, who is the project manager of the TUBITAK (The Scientific and Technological Research Council of Turkey) 1001 project (project no: 214M132, 'Smart nanoparticles for medical applications'), for which I worked as a scholar and also the subject of my thesis, for his suggestions, encouragement, support and guidance in writing the thesis. He was always behind me with his technical knowledge and advices during my thesis study.

I would like to express my gratitude to Assoc. Prof. Dr. Ali Kılıç for his expanding academic horizons and for his all kind suggestions, helpfulness and patience in my studies.

I would like to express that I am very grateful to Senior Scientist Dr. Smagul Karazhanov for his support, help and understanding to me. He was always patient and understanding.

I would like to thank Elvan Aydın for her guidance, endless helpfulness and morale in my work, she was always helpful.

I would like to thank my lab mate Farnoud Khakzad and Berat Keçeci for their friendship and helpfulness. I would also like to thank Selim Parlakyiğit for his assistance throughout my work, he was always patient and helpful.

In addition many thanks to Mehmet Çalışır and Emine Canbay for their helpfulness in SEM analyzes.

I would like to express my gratitude to my dear family for their endless love, great support, understanding of patience, encouragement and being by my side in all circumstances.

February 2021

Ayşesimay Çetin
Food engineer

TABLE OF CONTENTS

Page

FOREWORD ..... **ix**
TABLE OF CONTENTS ..... **xi**
ABBREVIATIONS ..... **xiii**
LIST OF SYMBOLS ..... **xv**
LIST OF TABLES ..... **xvii**
LIST OF FIGURES ..... **xix**
SUMMARY ..... **xxiii**
ÖZET ..... **xxv**
1. INTRODUCTION **1**
1.1 Purpose of Thesis 1
1.2 Literature Review 2
1.2.1 Treatment methods of cancer 2
1.2.1.1 Chemotherapy 2
1.2.1.2 Immunotherapy 3
1.2.1.3 Radiation therapy 3
1.2.1.4 Surgery 3
1.2.1.5 Hyperthermia therapy 4
1.2.1.6 Nano-magnetic hyperthermia (NMH) 5
1.2.2 Introductıon of magnetic nanoparticles 6
1.2.2.1 Nanomagnetism 7
1.2.2.2 Heating mechanism of magnetic nanoparticles 8
1.2.3 Fabrication methods for magnetic nanoparticles 10
1.2.3.1 Microemulsion method 10
1.2.3.2 Thermal decomposition method 10
1.2.3.3 Hydrothermal method 11
1.2.3.4 Co-precipitation method 11
1.2.4 Functionalization for surface of magnetic nanoparticles 13
1.2.5 Importance of particle size for magnetic nanoparticles 14
2. MATERIALS **17**
3. METHODS **19**
3.1 Core Synthesizing 19
3.2 Surface Coating of Superparamagnetic Nanoparticles 21
3.2.1 Oleic acid coating 21
3.2.2 Silica coating and amination of the superparamagnetic nanoparticles 21
3.2.3 Production process for $HAuCl_4$ 21
3.2.4 Gold coating and gold nanoparticles 24
3.2.5 PEG coating 25
3.3 Characterisation Techniques of Magnetic Nanoparticles 26
3.3.1 Scanning electron microscopy (SEM) 26
3.3.2 Fourier transform infrared spectroscopy (FTIR) 26

3.4 Heating Experiments of Superparamagnetic Nanoparticles 26
3.4.1 Adjusting of nanoparticles for heating experiment 26
3.4.2 Preparation of NP/agarose samples 27
3.4.3 Heating experiment set up 28
4. RESULTS AND DISCUSSION 33
4.1 Characterization of Superparamagnetic Nanoparticles 33
4.2 The Results of Magnetic Heating Experiments 37
5. CONCLUSIONS 49
REFERENCES 51
APPENDICES 61
CURRICULUM VITAE 81

ABBREVIATIONS

AC : Alternating current

ASC : Amination-functionalized Silica-coated core

AMF : Alternating magnetic field

APTMS : 3-Aminopropyltrimethoxy-silane

AuNPs : Gold nanoparticles

CT : Computed tomography

DNA : Deoxyribonucleic acid

EDX : Energy dispersive X-Ray

FTIR : Fourier transform infrared spectroscopy

GASC : Gold coated on Amination-functionalized Silica-coated core

MNP : Magnetic nanoparticle

MRI : Magnetic resonance imaging

NMH : Nano magnetic hyperthermia

NPs : Nanoparticles

PEG : Polyethylene glycol

PET : Positron emission tomography

PGASC : PEG coated on Gold coated on Amination-functionalized Silica coated core

SAR : Specific absorption rate

SC : Silica-coated core

SEM : Scanning electron microscope

SPIONs : Superparamagnetic iron oxide nanoparticles

TEOS : Tetraethyl orthosilicate

TUBITAK : The Scientific and Technological Research Council of Turkey

TurkStat : Turkish Statistical Institute

TUIK : Türkiye İstatistik Kurumu

US : Ultrasound

VSM : Vibrating sample magnetometer

LIST OF SYMBOLS

K	: The anizotropi constant
T	: Temperature
V_M	: Volume of particle
V_H	: Hydrodynamic particle volume
η	: Viscosity of the carrier liquid
f	: Frequency of applied AC magnetic field
k	: Boltzmann constant
τ	: Effective magnetic relaxation time
τ_B	: Brownian magnetic relaxation time
τ_N	: Neel magnetic relaxation time
τ_0	: 10^{-9} s
P	: Heat dissipation value
μ_0	: Permeability of free space
x^n	: AC magnetic susceptibility (imaginary part)
H^2apply	: Strength of applied AC magnetic field

LIST OF TABLES

Page

Table 3.1: Specifications of induction generator. **31**
Table 4.1: The list of materials abbreviation. **33**
Table 4.2: FTIR bands in literature. **33**
Table 4.3: SEM results. **37**
Table 4.4: The seconds given in the table is the time that the sample reaches 42°C.The summary table of Figure 4.5 and Figure 4.6 ..... **38**
Table 4.5: The seconds given in the table is the time that the sample reaches 42°C.The summary table of Figure 4.7 and Figure 4.8 ..... **39**
Table 4.6: The sequence of 'surface coating steps' when the samples reaching at 42°C in agar phantom. The seconds given in the table is the time that the sample reaches 42°C. This table summary about Figure 4.6 and Figure 4.9, Figure 4.10, Figure 4.11 and Figure 4.12. ..... **41**
Table 4.7: The sequence of 'surface coating stages' when the samples reaching at 42°C in water media. The seconds given in the table is the time that the sample reaches 42°C. This table about between Figure 4.13 and Figure 4.17. ..... **43**
Table 4. 8: The sequence of 'SPIONs type' when the samples reaching at 42°C in water media. The seconds given in the table is the time that the sample reaches 42°C. This table about between Figure 4.18 and Figure 4.21. **45**

LIST OF FIGURES

Page

Figure 1.1 **:** MNPs are injected, afterwards exposed to AMF to generate the desired heat in the targeting tumor [28]. **..... 6**

Figure 1.2 **:** Magnetic dipoles arrangement and movement under AMF and absence magnetic [32]. **..... 8**

Figure 1.3 **:** Illustrating Neel and Brownian relaxation after application ıf the magnetic filed B [3]. **..... 9**

Figure 1.4 **:** Solution ph effection on sizes of Fe3O4 NPs [47]……..**12**

Figure 1.5 **:** Reaction temperature effection on sizes of Fe3O4 NPs [47]. **..... 12**

Figure 1.6 **:** Stirring rate effection on sizes of Fe3O4 NPs [47]. **..... 13**

Figure 1.7 **:** (a) SPIONs core (b) silica coating (c) amination (d) gold decoration (e) gold shell coating [63]. **..... 14**

Figure 1.8 **:** Approximative NPs sizes that appear to be most suited for (a) tumor penetration, (b) tumor accumulation, and (c) AMF-Neel relaxation-driven hyperthermia. Also shown are the size ranges for (d) making stealth iron oxide particles for hyperthermia, and (e) particles size needed for magnetic field capture [28]. **..... 15**

Figure 3.1 **:** The solution for core NPs synthesis from left to right respectively : NaOH, $FeCl_3$, $FeCl_2$, $Sr(NO_3)$**. 19**

Figure 3.2 **:** Waiting process of NPs on magnet**. 20**

Figure 3.3 **:** End of the washing and clarifying of the NPs. **..... 21**

Figure 3.4 **:** Purification set up for $HauCl_4$ production. **..... 22**

Figure 3.5 **:** The residue on the beaker after purification process…….. **23**

Figure 3.6 **:** After adding distile water on the residue. **..... 23**

Figure 3.7 **:** All process returns to the beginning and obtain again pure gold powder (right side), if purification temperature more than 110°C. **..... 24**

Figure 3.8 **:** Gold colloidal solution after added 1% (w/v) sodium citrate solution. **..... 24**

Figure 3.9 **:** Color change from pale yellow to transparent after added potassium carbonate solution on %1 $HAuCl_4$ **.....25**

Figure 3.10 **:** Preparation of agarose/NPs mixture. **..... 27**

Figure 3.11 **:** NPs/agarose sample in the glass vessel after agarose gel became hardened……..**28**

Figure 3.12 **:** Optris CF-4 laser thermometer……**28**

Figure 3.13 **:** Receiving heating data with the Compact Connect Program**. 29**

Figure 3.14 **:** Transducer. **..... 29**

Figure 3.15 **:** Osciloscope**..... 30**

Figure 3.16 **:** Geometry of the helical coil that used in heating experiments**. 30**

Figure 3.17 **:** Dimensions of helical coil**. 30**

Figure 3.18 : Heating experimental set up with whole equipments: (1) Computer with Compact Connect Programme, (2) laser thermometer, (3) oscilloscope, (4) thermal camera, (5) PLC for laser thermometer, (6) thermometer, (7) black box for magnetic field and (8) induction generator. **31**
Figure 4.1 : FTIR spectra for Fe_C, Fe_SC, Fe_ASC, Fe_GASC (Fe_PGASC is omitted). **34**
Figure 4.2 : FTIR spectra for Mn_C, Mn_SC, Mn_ASC, Mn_GASC and Mn_PGASC..... **35**
Figure 4.3 : FTIR spectra for Mg_C, Mg _SC, Mg _ASC, Mg _GASC and Mg_PGASC. **35**
Figure 4.4 : FTIR spectra for Sr_C, Sr _SC, Sr _ASC, Sr _GASC and Sr _PGASC **36**
Figure 4.5 : Heating curves of Fe_C, Mg_C, Mn_C, Sr_C in water media as % 0.1 (v/v) equal volume ratio at 5 kw. **38**
Figure 4.6 : Heating curves of Fe_C, Mg_C, Mn_C, Sr_C in agar phantom as % 0.1 (v/v) equal volume ratio at 5 kw. **38**
Figure 4.7 : Heating curves of Mg_C with different concentration in water at 5 kw. **40**
Figure 4.8 : Heating curves of Mg_C with different concentration in agar phantom at 5 kw. **40**
Figure 4.9 : Heating curves of Fe_SC, Mg_SC, Mn_SC, Sr_SC in agar phantom as % 0.1 (v/m) equal ratio at 5 kw. **41**
Figure 4.10 : Heating curves of Fe_ASC, Mg_ASC, Mn_ASC, Sr_ASC in agar phantom as % 0.1 (v/m) equal ratio at 5 kW. **42**
Figure 4.11 : Heating curves of Fe_GASC, Mg_GASC, Mn_GASC, Sr_GASC in agar phantom as % 0.1 (v/m) equal ratio at 5 kW **42**
Figure 4.12 : Heating curves of Fe_PGASC, Mg_PGASC, Mn_PGASC, Sr_PGASC in agar phantom as % 0.1 (v/m) equal ratio at 5 kW. **42**
Figure 4.13 : Heating curves of Fe_C, Mg_C, Mn_C, Sr_C in water media as % 0.1 (v/m) equal ratio at 5 kW. **43**
Figure 4.14 : Heating curves of Fe_SC, Mg_SC, Mn_SC, Sr_SC in water media as % 0.1 (v/m) equal ratio at 5 kW **44**
Figure 4.15 : Heating curves of Fe_ASC, Mg_ASC, Mn_ASC, Sr_ASC in water media as % 0.1 (v/m) equal ratio at 5 kW **44**
Figure 4.16 : Heating curves of Fe_GASC, Mg_GASC, Mn_GASC, Sr_GASC in water media as % 0.1 (v/m) equal ratio at 5 kW **44**
Figure 4.17 : Heating curves of Fe_PGASC, Mg_PGASC, Mn_PGASC, Sr_PGASC in water media as % 0.1 (v/m) equal ratio at 5 kW **45**
Figure 4.18 : Heating curves of Fe_C, Fe _SC, Fe _ASC, Fe _GASC, Fe _PGASC in water media as % 0.1 (v/m) equal ratio at 5 kW **46**
Figure 4.19 : Heating curves of Mn_C, Mn_SC, Mn_ASC, Mn_GASC, Mn_PGASC in water media as % 0.1 (v/m) equal ratio at 5 kW **46**
Figure 4.20 : Heating curves of Mg_C, Mg_SC, Mg_ASC, Mg_GASC, Mg_PGASC in water media as % 0.1 (v/m) equal ratio at 5 kW **46**
Figure 4.21 : Heating curves of Sr_C, Sr _SC, Sr _ASC, Sr _GASC, Sr _PGASC in water media as % 0.1 (v/m) equal ratio at 5 kW. **47**
Figure A.1 : SEM images of Fe_C **63**
Figure A.2 : SEM images of Fe_SC **63**
Figure A.3 : SEM images of Fe_GASC **64**
Figure A.4 : SEM images of Mg_C **64**

Figure A.5 : SEM images of Mg_SC……..**65**
Figure A.6 : SEM images of Mg_GASC **65**
Figure A.7 : SEM images of Mn_C **65**
Figure A.8 : SEM images of Mn_SC **66**
Figure A.9 : SEM images of Mn_GASC **67**
Figure A.10 : SEM images of Sr_C **67**
Figure A.11 : SEM images of Sr_SC **68**
Figure A.12 : SEM images of Sr_GASC **68**
Figure B.1 : EDX of Fe_C **69**
Figure B.2 : EDX of Fe_SC **70**
Figure B.3 : EDX of Fe_GASC **71**
Figure B.4 : EDX of Mg_C **72**
Figure B.5 : EDX of Mg_SC **73**
Figure B.6 : EDX of Mg_GASC **74**
Figure B.7 : EDX of Mn_C **75**
Figure B.8 : EDX of Mn_SC **76**
Figure B.9 : EDX of Mn_GASC **77**
Figure B.10 : EDX of Sr_C **77**
Figure B.11 : EDX of Sr _SC **79**
Figure B.12 : EDX of Sr_GASC **80**

FABRICATION OF MULTI-COMPONENT SUPERPARAMAGNETIC NANOPARTICLES AND MAGNETIC HEATING PERFORMANCE FOR HYPERTHERMIA CANCER THERAPY

SUMMARY

Nowadays, cancer has become a major public health problem worldwide. It is known that 19.3 million new cancer cases and approximately 10 million cancer deaths occurred worldwide in 2020 alone. The TUIK 2020 report, the cancer is in second place with 80,186 people in Turkey ranking of causes of death.

Traditional methods such as chemotherapy, radiotherapy and surgery do not give highly successful results in cancer stages that have spread in the body. These treatment methods carry fatal risks by damaging healthy tissues depending on the treatment method in the patient. For this reason, various treatment methods have been developed that are expected to affect only damaged tissue.

Hyperthermia is one of the methods developed for this purpose. Multilayer functional superparamagnetic nanoparticles (NPs) are used in the method, which can be used in medical imaging and treatment applications. With these NPs, it is tried to develop the use of optical and magnetic methods for both diagnosis and treatment of cancer. Thanks to a dielectric shell coated on the NPs, its agglomeration can be prevented, and thanks to an organic shell coated on it, its properties such as biocompatibility and stability can be increased, as well as various molecule adhesion capabilities for treatment purposes can be given to the surfaces of the NPs. In addition to the magnetic properties of these NPs, it will be possible to heat them with the near infrared (NIR) laser to be applied due to their surface plasmon resonance properties.

Basically in this method; It is aimed to; (a) reach the denaturation temperature (42ºC) of the cancer cells by applying an alternative magnetic field that will affect only the tumor area, and (b) the malignant cells are destroyed by heating while the other healthy tissues remain stable. In this way, the side effects that occur in traditional methods are tried to be minimized.

The two most important factors determining the use of magnetic NPs in hyperthermia therapy are; (a) the applied NPs must have a high ability to heat the cancerous tissue to the desired temperature and (b) heating should be limited only to the cancerous tissue. These two factors can be achieved by having excellent magnetic properties that can reach the target temperature by using a small amount of NPs in the target tissue. For this reason, the type of magnetic NPs used and their magnetic heating performance are of great importance.

Studies on various NPs such as Fe_3O_4, $MnFe_2O_4$ are quite common, but it becomes impossible to compare the experimental results due to the different methods and

different environmental conditions determined for NPs fabrication in the studies. Therefore, more research is needed to make hyperthermia treatment available.

In the thesis, in the first part, Fe_3O_4, $MgFe_2O_4$, $MnFe_2O_4$ and $SrFe_{12}O_{19}$ NPs were synthesiszed as cores. Later, their outher surface was first coated with SiO_2 layer, functionalized with amination, then decorated via Au NPs and consequently the outer surface of overall NPs will be coated via PEG.

After each coating, the NPs have been characterized using FTIR, SEM and EDX. Heating process was carried out under AMF, using induction generator, in water and in agar according to the rate calculation of 0.1% (v/m) of the produced NPs.

According to the results of the heating tests, among all samples, $SrFe_{12}O_{19}$ NPs showed the lowest and $MgFe_2O_4$ NPs showed the highest heating performance among all samples in the tests where different core types were compared.

According to the heating results comparing the different coating stages, the aminated NPs gave the fastest warming result among the other coating stages.

Comparing different coating steps, PEG coated samples gave the slowest heating result in the heating results. In addition, the heating performance of gold-coated samples, which is the previous coating step from PEG, is very close to that of PEG coated samples and gave the second lowest performance.

As a result, our study has shown that different coating stages and NPs differences change the heating performance of superparamagnetic NPs. Although there are many studies of magnetic NPs in the literature, the effects of different types of magnetic NPs on the heating performance of different coating stages of these NPs were compared under standardized laboratory conditions. It is possible to say that this study, which is carried out with easily accessible and economical laboratory materials, is illuminating for future researches related to the subject.

HİPERTERMİ KANSER TERAPİSİ İÇİN ÇOK BİLEŞENLİ SÜPERPARAMANYETİK NANOPARTİKÜLLERİN ÜRETİMİ VE MANYETİK ISINMA PERFORMANSI

ÖZET

Günümüzde kanser dünya çapında önemli bir halk sağlık sorunu haline gelmiştir. Dünya genelinde, sadece 2020 yılında, 19.3 milyon yeni kanser vakası ve yaklaşık 10 milyon kanser ölümünün meydana geldiği bilinmektedir. TUİK 2020 raporunda ise kanser, Türkiye'de ölüm nedenleri sıralamasında 80.186 kişi ile ikinci sırada yer almaktadır.

Kemoterapi, radyoterapi ve cerrahi gibi geleneksel yöntemler vücutta yayılma göstermiş kanser evrelerinde yüksek oranda başarılı sonuçlar vermemektedir. Bu tedavi yöntemleri hastada tedavi yöntemine bağlı olarak sağlıklı dokulara da hasar vererek ölümcül riskler taşımaktadır. Bu sebeple sadece hasarlı dokuya etki etmesi beklenen çeşitli tedavi yöntemleri geliştirilmiştir.

Hipertermi bu amaçla geliştirilen yöntemlerden biridir. Yöntemde, tıbbi görüntüleme ve tedavi amaçlı uygulamalarda kullanılabilecek çok katmanlı fonksiyonel süperparamanyetik nanopartiküller (NP) kullanılmaktadır. Bu NP' ler ile, kanserin hem teşhisi hem de tedavisi için optik ve manyetik yöntemlerin kullanımı geliştirilmeye çalışılmaktadır. NP' lere kaplanan dielektrik bir kabuk sayesinde topaklanmaları engellenebilir ve organik bir kabuk sayesinde ise biyouyumluluk, kararlılık vb. özellikleri yanı sıra yüzeylerine tedavi amaçlı çeşitli molekül yapıştırılabilme kabiliyetleri kazandırılabilir. Bu NP' lerin manyetik özellikleri yanı sıra, yüzey plazmon rezonans özelliklerinden dolayı uygulanacak yakın kızılaltı (NIR) lazer ile de ısıtılmaları mümkün olabilecektir.

Bu yöntemde temel olarak; (a) sadece tümor bölgesine etki edecek alternatif manyetik alan uygulanarak kanser hücrelerinin denatürasyon sıcaklığına (42ºC) ulaşması ve (b) kötü huylu hücrelerin ısıtılarak yok edilirken diğer sağlıklı dokuların ise stabil kalması amaçlanmaktadır. Bu şekilde geleneksel yöntemlerde ortaya çıkan yan etkiler en aza indirgenmeye çalışılmaktadır.

Manyetik NP'lerin, hipertermi terapisinde kullanılmalarını belirleyen en önemli iki faktör; (a) uygulanan NP' lerin kanserli dokuyu istenilen sıcaklığa ısıtabilme kabiliyetinin yüksek olması ve (b) ısıtmanın sadece kanserli doku hacmi ile sınırlandırılmış olmasıdır. Bu iki faktör, hedef doku içerisinde NP' lerin az miktarda birikme konsantrasyonu ile dokuyu hedeflenen sıcaklığa ulaştırabilecek kadar mükemmel manyetik özelliklere sahip olması ile sağlanabilir. Bu sebeple, kullanılan manyetik NP' lerin çeşidi ve manyetik ısınma performansı büyük ölçüde önem göstermektedir.

Fe_3O_4, $MnFe_2O_4$ vb. çeşitli NP' lerle ilgili çalışmalar oldukça yaygındır, fakat yapılan çalışmalarda NP üretimi için belirlenen metotlarının ve ortam şartlarının farklı olması deney sonuçlarının karşılaştırılmasını imkansız kılmaktadır. Bu nedenle hipertermiya tedavisinin kullanılabilir düzeyde olması için daha fazla araştırmaya ihtiyaç duyulmaktadır.

Bu çalışmada, süperparamanyetik NP çekirdekleri standartlaştırılmış yöntemler ile üretilip literatürde başarılı bulunan metotlar ile kaplanmıştır ve ardından karakterizasyon işlemlerine tabi tutulmuştur. Üretilen tüm NP çeşitleri ve uygulanan her bir kaplama katmanı için manyetik ısıtma performansları ayrı ayrı incelenmiştir.

Çalışmada öncelikle , NP çeşitlerinin üretimi ve çeşitli kaplamalar ile modifikasyonu yapılmıştır. Bunun için üretimin ilk aşamasında, süperparamanyetik güçlerinin yüksek olması, üstün ısınma kabiliyetleri ve literatürde oldukça başarılı sonuçlar göstermesi gibi özellikleri sebebiyle seçilen Fe_3O_4, $MnFe_2O_4$, $MgFe_2O_4$, $SrFe_{12}O_{19}$ NP çekirdekleri çökeltme metodu ile üretilmiştir. Geçmişteki deneyimlerden bilindiği üzere; Fe_3O_4 NP çekirdekleri hızlı oksitlendiği için sadece bu NP' ün sentezleme aşamasında oleik asit kaplaması yapılmıştır. Üretimin ikinci aşamasında, bu 4 farklı NP çekirdekleri topaklanmayı önleyici dielektrik bir kabuk olarak SiO2 ile kaplanmıştır. Üretimin üçüncü aşamasında, silika kaplanan numuneler, altın kaplamaya uygun bir bağlanma yüzeyi sağlanması adına aminasyon işlemine tabi tutulmuştur. Üretimin dördüncü aşaması olan altın kaplama işlemine geçmeden önce, bu kaplamada kullanılacak ana madde olan $HauCl_4$ çözeltisi laboratuvar şartlarında üretilmiş, daha sonra ise bu çözelti ile NP' lere altın kaplama yapılmıştır. Biyouyumluluğu, kimyasal stabilitesi ve farklı fonksiyonel gruplara bağlanabilme kabiliyetini arttırmak amacıyla yapılan altın kaplama sonrası, NP' lerin kan dolaşımında kalma süresinin artması, biyouyumlu olması ve kararlılığının artması için, üretimin son aşaması olan PEG kaplama işlemi yapılmıştır.

NP üretimi bittikten sonra, her kaplama sonrasında elde edilen NP' ler FTIR (Fourier Dönüşümlü Infrared Spektrofotometre) ve SEM (İngilizce: Scanning Electron Microscope) kullanılarak karakterize edilmiştir. FTIR sonuçlarına göre tüm kaplama aşamalarının gerçekleştiğinin göstergesi olan piklere ulaşılmıştır. SEM ile NP çapları incelenmiş ve ayrıca altın kaplı numunelerin EDX (İngilizce: Energy Dispersive X-ray Spectroscopy) sonuçlarıyla istenen altın içerikleri elde edilmiştir.

Çalışmanın son aşamasında ise, üretilen NP' lerin % 0.1 (v/m)' lik oran hesabına göre su içerisinde ve agar içerisinde olmak üzere ısıtma işleminin yapılacağı 2ml'lik cam kapta ayrı ayrı numuneleri hazırlanmıştır. Hazırlanan numuneler laboratuvar şartlarında kurulan indüksiyon jeneratörü kullanılarak ısıtma deneylerine tabi tutulmuştur.

Isıtma testlerinin sonuçlarına göre, farklı çekirdek tiplerinin karşılaştırıldığı testlerde tüm numuneler arasında $SrFe_{12}O_{19}$ NP' leri en düşük, $MgFe_2O_4$ NP' ü ise en yüksek ısınma performansını göstermiştir.

Farklı kaplama aşamalarının karşılaştırıldığı ısıtma sonuçlarına göre ise, diğer kaplma aşamaları arasında en hızlı ısınma sonucunu aminasyon işlemi yapılmış NP' ler vermiştir. Bu şaşırtıcı ve sezgisel olmayan bir sonuçtur. Bir şekilde aminasyon işlemi yapılmış örnekler çekirdek tipinden bağımsız olarak tüm çok bileşenli örneklerde ısınma gücünü arttırıcı yönde etki göstermiştir. Şimdiye kadar bilinen dahilinde, elde edilen bu çalışma sonuçlarıyla literatürde daha önce karşılaşılmamıştır.

Farklı kaplama aşamalarının karşılaştırıldığı ısıtma sonuçlarında en yavaş ısınma sonucunu ise son katman olan PEG kaplı numuneler vermiştir. Buna ek olarak PEG' den bir önceki kaplama aşaması olan altın kaplanmış numunelerin ısınma performansı, PEG kaplı numunelerinkine oldukça yakın ve en düşük ikinci performansı vermiştir.

Literatürde altın kaplamanın numunenin ısınma performansını göreceli olarak arttırdığı gözlenen çalışmalar vardır, bizim çalışmamızda ise ısınma performansını göreceli olarak azaltmış olmasıyla ilgili olarak; (a) NP' lerin boyutlarının, kaplama kalınlıklarının farklı olması ve (b) ısınma deneylerine yönelik hazırlanan karışımların aynı miktarda NP içermemesi gibi standardizasyonu etkileyen parametrelerin varlığından söz edilebilir. Bunun yanı sıra, çalışmada altın kaplamanın varlığını kanıtlamak için EDX ile numuneler incelenmiş ve hepsinde altın içeriğine rastlanmıştır, fakat altın kaplama işleminden sonra yapılan yıkama işleminin yetersiz olma ihtimali sebebiyle, altın kaplama başarısız olduğu halde EDX piklerinde altın gözükmüş olma ihtimali yadırganamaz. Kaplamaların başarısı ve NP boyutları ile ilgili daha güvenilir bir sonuç elde edilmesi için ayrıca TEM ile karakterizasyon çalışması yapılması önerilmektedir.

Sonuç olarak çalışmamız farklı kaplama aşamalarının ve NP farklılıklarının süperparamanyetik NP' lerin ısınma performansını değiştirdiğini göstermiştir. Literatürde birçok farklı manyetik NP' e ait çalışmanın olmasına karşın bu çalışma ile standardize edilmiş laboratuvar koşullarında farklı tipte manyetik NP' ler ile bu NP' lerin farklı kaplama aşamalarının ısınma performansına etkisi karşılaştırılmıştır. Kolay ulaşılabilir ve ekonomik laboratuvar malzemeleriyle gerçekleştirilen bu çalışmanın konuyla bağlantılı gelecek araştırmalar için aydınlatıcı olduğunu söylemek mümkündür.

1. INTRODUCTION

Despite various treatment methods, cancer is still one of the major health problems today. According to the data in 2016, 80.577 people died due to cancer are also turkey is the leading cause of death in the United States ranks second area. According to statistical data, cancer death rate increased by 22% from 1990 to 2000. According to statistics, deaths due to cancer will be around 15.4 million in the 2020s [1]. It carries the risk of killing living tissues in traditional cancer treatment methods. In order to eliminate this risk, targeted treatment methods are being investigated by using nanotechnology. With targeted treatment methods, it is aimed to affect only the cancerous tissue without damaging the healthy tissue. In targeted therapies, SPIONs are one of the promising cancer treatment methods due to the easy control of the magnetic core and their ability to generate enough heat to destroy the tumor site, and can be used as an adjunct treatment method with chemotherapy and radiotherapy [2-4]. SPIONs can be functionalized to change their in vivo behavior or adapt to desired size, surface properties, desired magnetic properties [5]. In hyperthermia therapies, which is the process of heating the targeted area by exposing the cancerous tissue to the AMF by means of functionalized SPIONs, it is aimed to treat only the cancerous area by protecting the healthy tissue [6]. It is a cancer treatment method that has attracted much attention in biomedical treatment research in the literature and is called green therapy [7].

1.1 Purpose of Thesis

In this study, four different SPIONs core, namely Fe_3O_4, $MnFe_2O_4$, $MgFe_2O_4$, $SrFe_{12}O_{19}$ were produced using the co-precipitation method, and then a dielectric-SiO2 nano layer to prevent agglomeration, a functional layer with amination to hold the gold coating, decoration with Au NPs and finally coating with PEG to increase the biocompatibility of the outer surfaces of these cores were carried out, respectively [8-11].

In our study firstly, in heating experiments under AMF, the change in the heating behavior under AMF of the produced superparamagnetics was observed with the increase in concentration in water media and agar phantom. Secondly, in order to use NPs at the lowest possible dosages in the hyperthermia therapy, it has been tested to obtain high heating performance by using the least amount of NPs as possible. Therefore, the heating performance of Fe_3O_4, $MnFe_2O_4$, $MgFe_2O_4$, $SrFe_{12}O_{19}$ NPs at low concentrations was investigated. Thirdly, the effect of different coating types on the heating performance of NPs was investigated.

1.2 Literature Review

1.2.1 Treatment methods of cancer

The diagnosis of cancer and choosing the right treatment method directly affects of the treatment of the patient and the prolongation of the patient's life.

The treatment methods used vary according to the type of cancer. Commonly used treatment methods are chemotherpy, immunotherapy radiation therpy, surgery and hyperthermia therapy [12].

1.2.1.1 Chemotherapy

Although chemotherapy means "drug therapy", it is the term mainly used for treatment using cancer drugs that affect cancer cells. The goals of chemotherapy may differ according to the type of cancer, the shape of the cancer cells. Thanks to chemotherapy drugs, the fast division mechanisms of cancer cells are destroyed or cell division stops [13].

Cancer treatment with chemotherapy method has been used in medicine for many years and successful treatment results have been obtained [14].However, since the immune system of the patient lowers, damages the nerves in the hands and feet, affects the patient's appetite, can affect the way various organs in the body work negatively, and such damage is permanent in some patients, new targeted treatment methods have been developed [13]. Many researches such as new drug combinations, targeted liposomal and monoclonal antibody therapy, chemo-protective agents, hematopoietic

stem cell transplantation and agents are carried out to get rid of the destructive effects of chemotherapy [14].

1.2.1.2 Immunotherapy

In immunotherapy, an immune system response against cancer cells are created in the body by using biological agents. Normal signals promoting tumor growth are mimicked.

These biological agents, including interferons, interleukins, cytokines, endogenous angio-inhibitors and antigens, are produced in the laboratories [14].

1.2.1.3 Radiation therapy

In radiation therapy, radiation rays are used for cancer treatment by affecting the DNA of cancer cells. Three years after the discovery of X-Rays in 1986, it was used in the diagnosis and treatment of cancer. There are two types of radiotherapy as external radiotherapy and internal radiotherapy. Radiation therapy affects healthy cells, but the repair mechanism resolves this negative effect.

Radiation therapy is still important cancer therapy methods, although radiation rays causes cancer. The duration of treatment depends on the location of the tumor in the body, the size and type of cancer [14,15].

1.2.1.4 Surgery

The surgical method is used to diagnose cancer by biopsy or to treat cancer by cutting the tumor. In this method, early detection of cancer and removal before it spreads to the body increases the success of treatment. It is a treatment method that is not sufficient alone in cancers that have spread to the body [16,17].

Getting a good result with this method depends on the stage of the cancer, the type of cancer, its location in the body and the general health of the patient [17]. With the advancement of medical technology in fields such as ultrasound (US), Computed tomography (CT), magnetic resonance imaging (MRI) and positron emission tomography (PET), less risky methods of eliminating the tumor without cutting it are

being investigated. Freezing cancer cells with liquid nitrogen or cutting tumor tissue using laser are some of these methods [14].

1.2.1.5 Hyperthermia therapy

Hyperthermia is a treatment approach applied by heating the unhealthy area above physiological temperatures in order to make cells more sensitive to damage cells, kill cells or help other treatments [18,19].

For healthy person, the body temperature varies between 36ºC-38ºC, this temperature may increase or decrease during the day. Most people can tolerate body temperature differences up to 40°C when hydrated sufficiently, but after this temperature, cells begin to die at temperatures around 42°C-43°C [20].

In general, for a successful treatment in hyperthermia therapy, the temperature of the tumor site is raised to the range 41°C-47°C. The temperature reached for a successful hyperthermia treatment depends on the duration of the treatment and the cell and tissue properties. With the rise in temperature, the permeability of the vessel within the tumor changes and causes irregular, weak blood flow, which causes tumor cells to be more sensitive than healthy cells. In addition, cells in the synthesis phase are the most sensitive cells to thermal therapy, so rapidly dividing cancer cells die more than normal in the treatment of hyperthermia [21,22].

Using NPs as hyperthermia agents is one of a kind approach to developing an effective hyperthermia method [18].

There are some important points for an effective hyperthermia treatment:

- ✓ Limited tumor areas give positive results in early treatment.
- ✓ It is difficult to maintain healthy cell areas and to affect only the tumor area
- ✓ When hyperthermia is applied, it is difficult to maintain a homogeneous temperature distribution in that area in case of changes in physiological factors (such as blood pressure) [6].

As a result of the researches, it has been proven that hyperthermia treatment is an important adjunct treatment, but standard treatment has not yet been reached [23].

1.2.1.6 Nano-magnetic hyperthermia (NMH)

One of the critical issues in the treatment of hyperthermia is to make homogeneous heat distribution in the tumor tissue. It is risky to have unheated areas inside the tumor area. For a good therapeutic approach, the temperature difference between tumor tissue and healthy tissue must be observed exactly. Nano magnetic hyperthermia (NMH) offers the solution required to create a temperature difference between the tumor area and healthy tissue. The basic principle in NMH method is based on magnetic energy losses of magnetic nanomaterials in the presence of an AMF. There are two main mechanisms in the NMH method: hysteresis losses and relaxation losses [18].

Various surface modifications are made to MNPs to prevent agglomeration, biocompatibility, and functionalization of NPs. In the case of hyperthermia using MNPs, the magnetic core of the NPs is modified with various coatings: stabilization is provided to prevent the magnetic fluid from agglomerating, modified with specific coatings for biocompatibility, different ligands are added to the surface to increase the functionality of the NPs [18,19].

After MNPs loaded into a tumor tissue are exposed to an AMF, specific magnetization processes take place and the magnetic polarities of the particles are rapidly reversed. The heating potential (SAR) of NPs is an important parameter that determines how much NPs should be loaded into the tumor area. The amount of heating given per unit mass and time after NPs are exposed to AC is called SAR (called heating potential) The size of the AMF, the properties and size of the MNPs, the spread of the tumor in the body, and the concentration of NPs in the tumor are factors that affect the heating of the treatment [23,24].

It is technically difficult to rise above 37.5°C in a specific targeted area. Approximately 1 W kg 1 SAR is estimated to cause an increase in temperature of 1ºC in the human body [25,26].

The volume of the tumor and how much heat is given to the tumor are critical in the treatment of hyperthermia. Heating 90% of the tumor to 43°C for 10 min gives two times faster results than applying radiotherapy treatment alone [16,27].

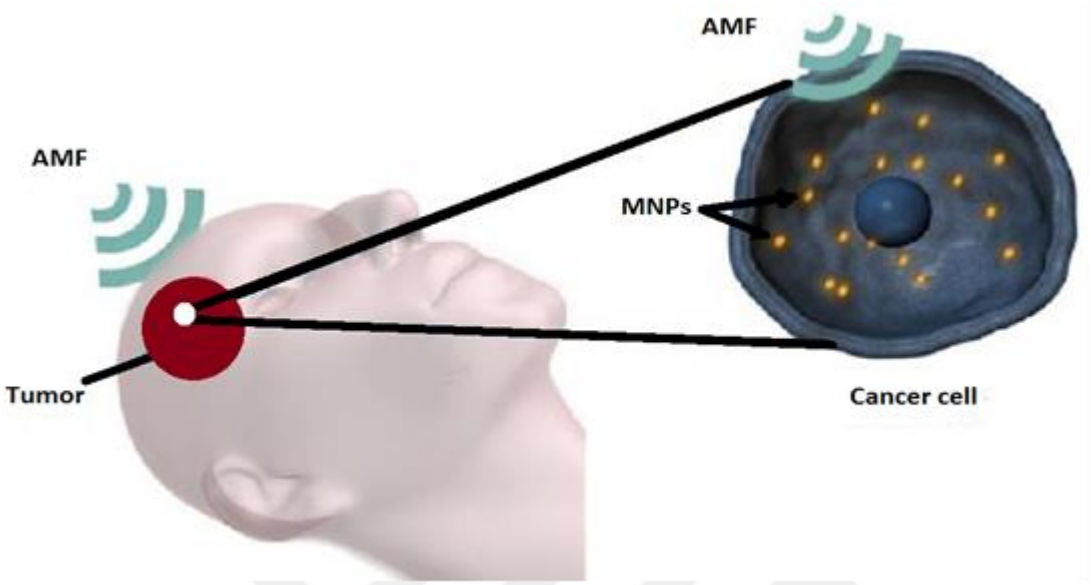

Figure 1.1 : MNPs are injected, afterwards exposed to AMF to generate the desired heat in the targeting tumor [28].

1.2.2 Introduction of magnetic nanoparticles

Iron oxide NPs generally have diameters smaller than 40 nm and are called superparamagnetic nanoparticles (SPIONs) [23].

The geometric properties of MNPs depend on interactions between particles, intra-particle magnetic interactions, magnetic interactions occurring between NPs and matrix material, and applied AMF interaction [29].

MNPs display different physical, biological and chemical properties according to their varying sizes (1-100nm) [19].

MNPs are used in various clinical applications due to their various physical properties such as being easy to manipulate, being used as an MRI contrast agent due to their effects on the T1 relaxation period, and being able to target thermal energy remotely and accurately to the desired area. Apart from these, it has many features such as easy

surface modification, high biocompatibility, small size, non-toxicity, injectability [19,30].

Applications of NPs in the medical field are suitable for use in areas such as the control and application of magnetic properties, cancer diagnosis and treatment. In addition, the use of MNPs in areas such as drug targeting, MRI contrast enhancement agents, nano biosensors and magnetic fluid hyperthermia is being investigated. The potential use of NPs in these areas varies according to the particle size, composition, structure and physicochemical properties of the NPs [19].

MNPs are generally coated with a biocompatible material to make them biocompatible, thus prolonging their life cycle in the bloodstream and preventing their accumulation in the body circulation. Biomolecules such as antibodies are added to the part of which active targeting is desired, and it is directed to the desired tissue [30].

Late diagnosis of cancer is an important factor that makes treatment difficult. With the application of MNPs, cancer can be detected early and adequate treatment can be provided [31].

In order to use MNPs in the treatment of hyperthermia, the heating power of NPs must be sufficient and the NPs must have a good stability. The fact that the NPs are superparamagnetic increases its stability, and the high saturation magnetization helps the NPs provide a good thermal energy. When the applied AMF is removed and the temperature of the block is exceeded, the SPIONs lose its magnetism [29].

1.2.2.1 Nanomagnetism

MNPs are affected by intrinsic and extrinsic parameters that affect magnetism. MNPs are classified as paramagnetic, diamagnetic, ferromagnetic, ferrimagnetic, antiferrimagnetic according to the movement of the inner dipole and the presence of the magnetic forehead applied externally. Figure 1.2 illustrate that magnetic dipole arrangement for Diamagnetics, Paramagnetics, Ferromagnetic, Ferrimagnetic and Antiferrimagnetic materials.

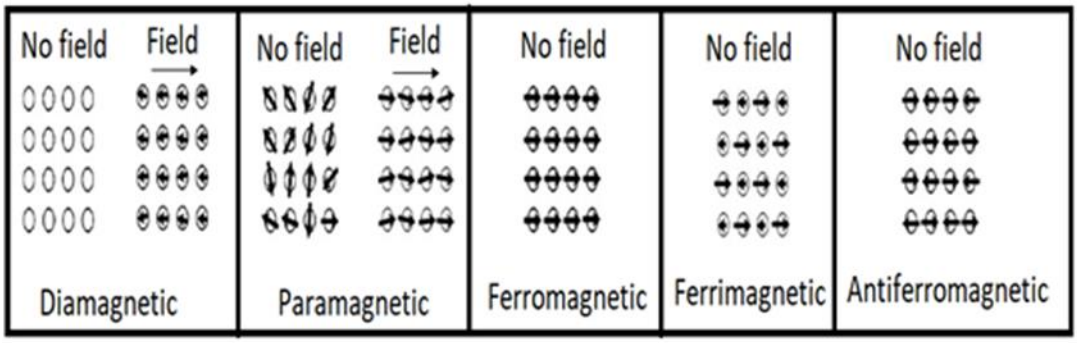

Figure 1.2 : Magnetic dipoles arrangement and movement under AMF and absence magnetic [32].

***Paramagnetics**:* For paramagnetic materials, there exist magnetic dipoles as showed in Figure 1.2, but these dipoles are aligned only onto application of an exterior magnetic field applied. In order to the equilize of the magnetic properties showed in Figure 1.2, the magnetization in the lack of an applied field express their basic character.

Diamagnetics: For diamagnetic materials in the lack of a magnetic field applied, magnetic dipoles are not existing. On the other hand, onto application of a field, the material fabricate a magnetic dipole that is directional opposite to that of the applied field; in this way, a material that has strong diamagnetic character is repulse by a AMF.

Ferromagnetic: It has net magnetic dipole moments even if there is no application of an external magnetic field.

***Ferrimagnetic and antiferrimagnetic**:* The atomic level magnetic dipole moments are like to those of ferromagnetic materials, on the other hand, adjacent dipole moments exist that are not oriented in parallel and effectively cancel or reduce, respectively.

1.2.2.2 Heating mechanism of magnetic nanoparticles

Hysteresis losses: It is defined as the heat generated from the energy losses that occur as a result of the periodic magnetization of ferromagnetic materials. Hysteresis losses are neglected because of the very small size of SPIONs, the energy required for heating to SPIONs basicly comes from relaxation losses [28].

Relaxation losses: It depends on the rotation of the magnetic vectors inside the particle (neel) or the rotation of the particle in the carrier fluid (brownian) when exposed to the external magnetic field . Figure 1.3 show that the MNPs orientation and their relaxation statuse after magnetic field B [33,34].

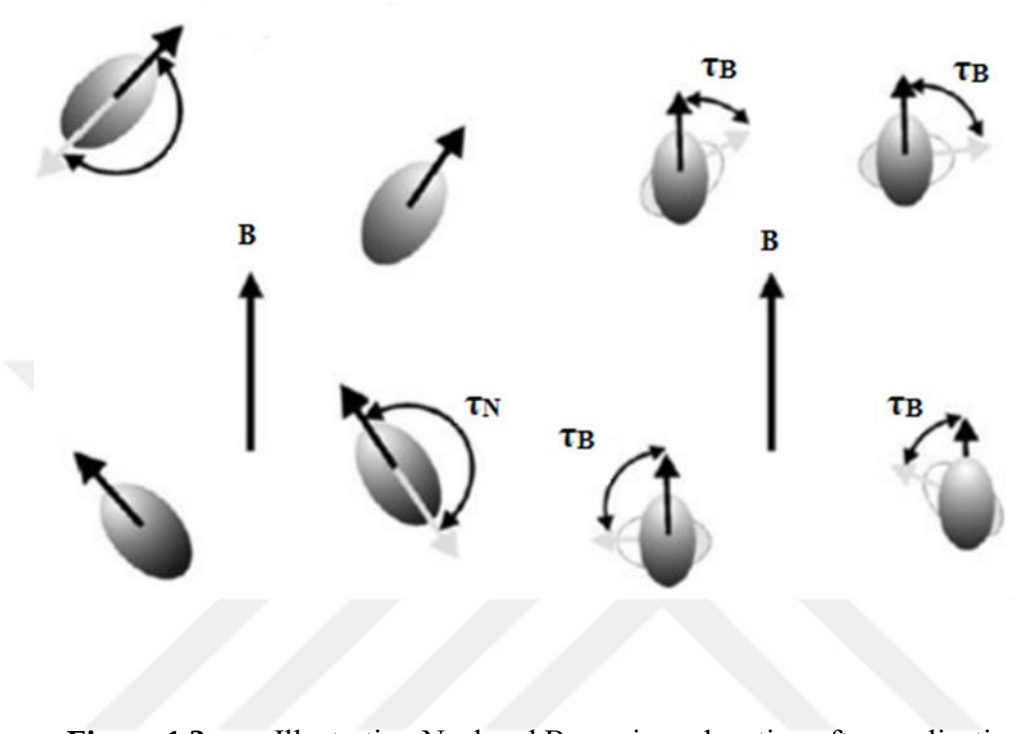

Figure 1.3 : Illustrating Neel and Brownian relaxation after application ıf the magnetic filed B [3].

The Neel (τ_N) and Brownian (τ_B) magnetic relaxation times of a MNPs are expressed in the belowing equations (1.1), (1.2), (1.3).

$$\tau_N = \tau_0 \,.\, exp\left({}^{K.V_M}/_{k.T}\right) \qquad (1.1)$$

$$\tau_B = {}^{3\,.\eta.V_H}/_{k.T} \qquad (1.2)$$

$$\tau = {}^{\tau_B.\tau_N}/_{\tau_B + \tau_N} \qquad (1.3)$$

$\tau_0 = 10^{-9}$ s, K the anizotropi constant, τ_N the Neel relaxation time, τ_B the Brown relaxation time the effective relaxation time, V_M the volume of particle, k the Boltzmann constant, T the temperature, η the viscosity of the carrier liquid and the V_H the hydrodynamic particle volume.

MNPs relaxation time depends on particle diameter. When the MNPs are applied to an AC magnetic field with time of magnetic reversals less than the magnetic relaxation times of NPs, heat is spread because of the delay in the relaxation of the magnetic vector. In this way , the heat dissipation value is obtained using the harmonic of both relaxations and their relative contributions depending on the NPs diameter. The heat dissipation (*P*) is showed by the following equation [34].

$$P = \mu_0 . x^n . f . H^2 apply \qquad (1.4)$$

P heat dissipation value, μ_0 permeability of free space, x^n AC magnetic susceptibility (imaginary part), $H^2 apply$ strength of applied AC magnetic field.

1.2.3 Fabrication methods for magnetic nanoparticles

1.2.3.1 Microemulsion method

In this method, the surfactant molecules and the oil phase co-precipitate with the small water pool embedded. Here, the surfactant creates the effect of trapping the molecule and limits the growth, nucleation and agglomeration of the particles [35-39].

It is a system that consists of two thermodynamically and isotropically stable immiscible liquids, water and oil phases, and an interface film of surfactant molecules. NPs can be synthesized in various morphologies, but a large amount of solvent is needed and the production efficiency is low [40].

1.2.3.2 Thermal decomposition method

In this method, organometallic precursors are decomposed under high temperature, and in this way, monodisperse and size control of NPs are obtained in high quality [28,40].

The main parameters determining particle diameter and morphology are the ratio of starting reagents. Besides, reaction temperature can be very effective for precise control of size and morphology in reaction time. One of the most important challenges in this method is to keep the heating rate constant during the period of nucleation and growth [28,41,42].

1.2.3.3 Hydrothermal method

It is a heterogeneous reaction that takes place in an water media under high pressure and high temperature conditions. It is possible to produce a wide variety of nano-structured materials with this method [35].

In this method, temperature and time are important parameters that affect the product [28,43].

1.2.3.4 Co-precipitation method

There are various studies on the production of MNPs for biomedical use by using co-precipitation method [44-50].

One of the most used methods of MNPs production. It is formed by the precipitation of various materials containing Fe^{+2}/Fe^{+3} ions and Sr^{+2}, Mg^{+2}, Mn^{+2} ions using various alkaline solutions. This method requires Fe^{+2}/Fe^{+3} ions and Sr^{+2}, Mg^{+2}, Mn^{+2} ions to be well protected and the pH value of the solution to be adjusted well [44-50]. The process takes place at room temperature or at a high temperature under an inert atmosphere. Parameters such as size, shape, composition of salts used in solution, ratio of Fe^{+2}/Fe^{+3} ions, reaction temperature, pH value, ionic strength, used concentration affect synthesis [44,45,51-53]

In the experiments, the structure and size of the NPs produced by changing the parameters such as the pH of the distilled water used in the precipitation method, the molar ratio and concentration of the material, temperature and mixing speed were checked [45,47,54-56].

Figure 1.4. it represents the effect of pH change on size of NPs. Figure 1.5. represents the effect of temperature change on NPs size. Figure 1.6. represents the effect of different stirring rate on NPs size.

Reaction temperature and time are lower than thermal decomposition and hydrothermal methods. In addition, since water is used as a solvent, it is environmentally friendly, besides, its reaction efficiency is high and scalable. However, size distribution is relatively narrow and shape control is not satisfying [40,42].

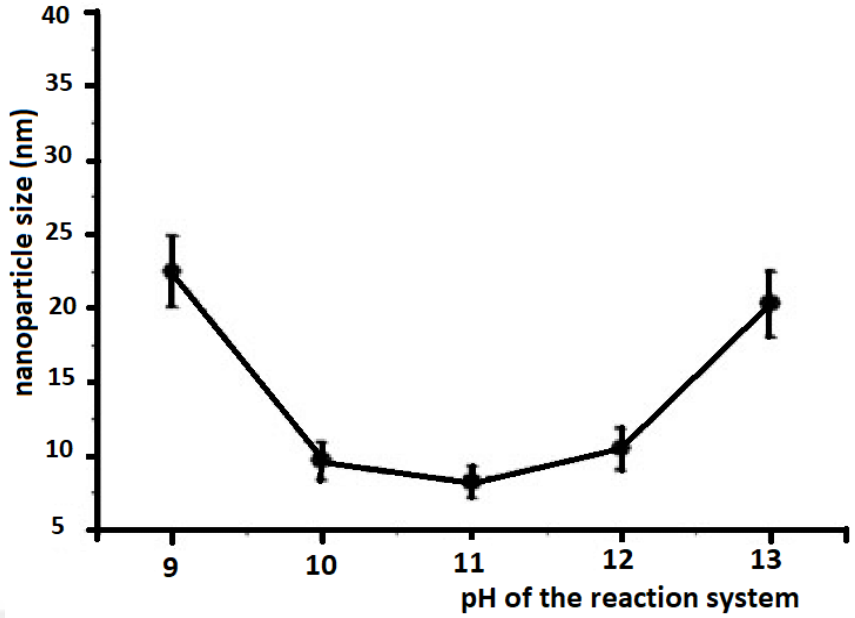

Figure 1.4 **:** Solution ph effection on sizes of Fe3O4 NPs [47].

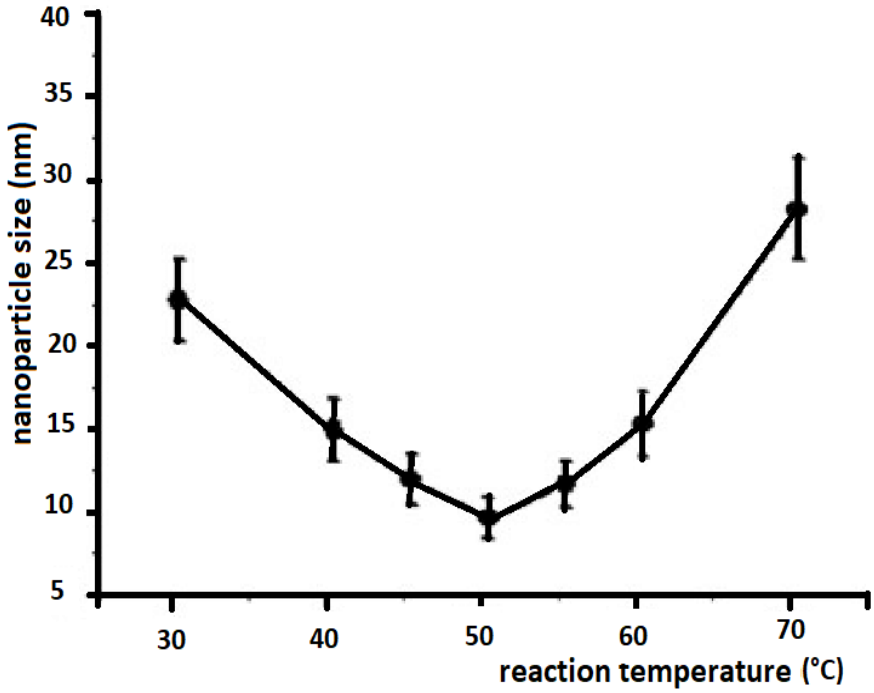

Figure 1.5 **:** Reaction temperature effection on sizes of Fe3O4 NPs [47].

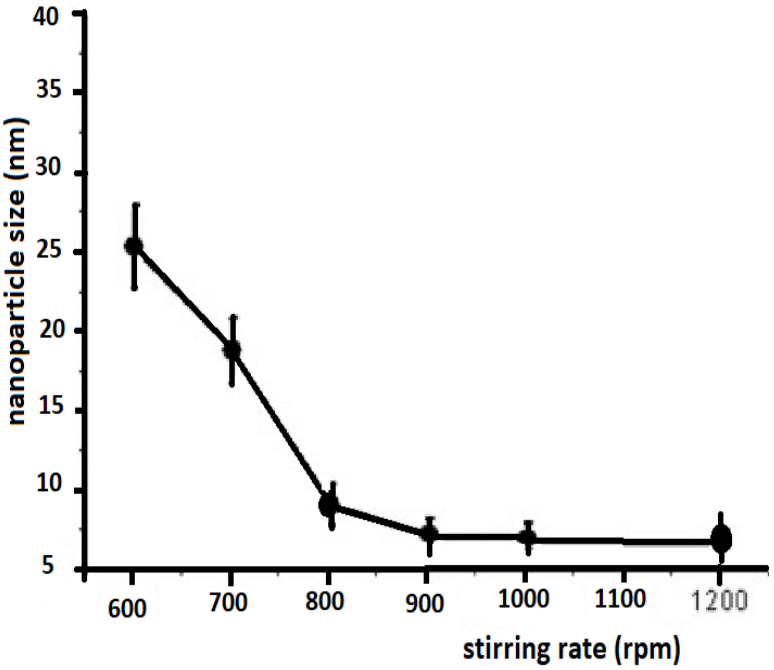

Figure 1.6 : Stirring rate effection on sizes of Fe3O4 NPs [47].

1.2.4 Functionalization for surface of magnetic nanoparticles

Studies have found that iron oxide core NPs accumulate in the Kupffer cells of the liver. To ensure the accumulation of NPs in the tumor region, the NPs must be covered with polymer material or placed inside the polymer shell. NPs with Fe^{+2} / Fe^{+3} oxide core shell are one of the popular productions to avoid such adverse situations [19,24].

In surface modifications to NPs for cancer treatments, oleic acid coating to prevent oxidation [57,58], silica coating to prevent agglomeration [59-72], amination process to prepare NPs for gold coating [63,73-76], gold coating process NPs to prevent body To make them nontoxic to organs [63,73-76,78-85], polymer coating [57,77,86-94] is apply to make NPs biocompatible with body organs and cells.

SPIONs can interact with the human immune system. In addition, depending on the type of synthesis method, aggregation may occur on the hydrophobic surface of the NPs. For such reasons, coating NPs with silica is a strong necessity. When NPs are coated with silica, surface ligands adhere more easily to MNPs surface due to the presence of silanol groups on the surface. In addition, silica coating provides stabilization of particles by increasing electrostatic repulsions between particles (in non-liquid dispersions) and preventing dipolar attraction (in liquid dispersions). For such reasons, it is one of the popular coatings for biomedical applications [42,95].

In order to stabilize Fe_3O_4 NPs and prevent oxidation, oleic acid coating is applied. In addition, adding N_2 gas during the reaction prevents oxidation [40].

Nano gold coating is biocompatible and allows different jewelery to be attached to the surface and also increases chemical stability. There are results in the researches that the heating performance of the gold-coated NPs is increased when it is heated under AMF [24,95].

It can be used in natural or synthetic polymers for coating MNPs. The most commonly used synthetic polymers are polyethylene glycol (PEG), polyvinyl alcohol (PVA), polyethyleneemine (PEI), polyvinylpyrrolidone (PVP). Among these polymers, PEG is water soluble and biocompatible. In some studies, it has been reported that PEG coating increases the circulation time of NPs in the blood and shows high solubility and stability in aqueous solution [43].

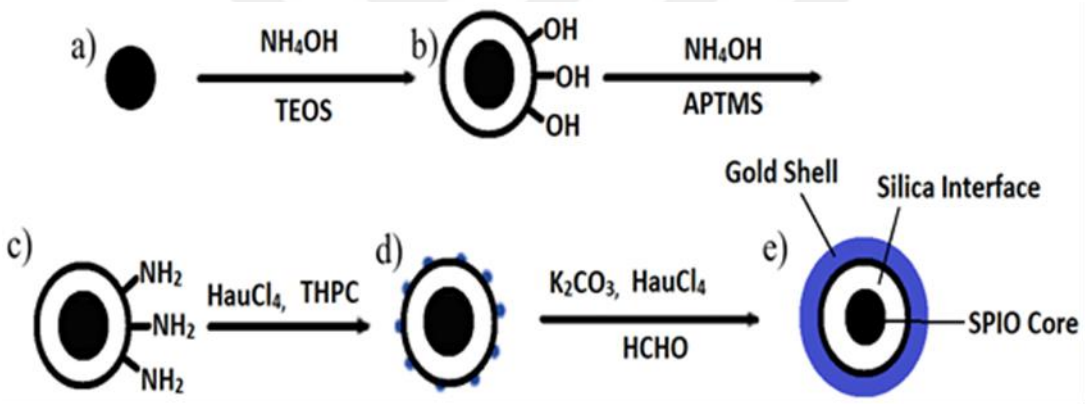

Figure 1.7 **:** (a) SPIONs core (b) silica coating (c) amination (d) gold decoration (e) gold shell coating [63].

Figure 1.7 show that SPIONs core fabrication and in the following its functionalization which includes silica coating, amination and gold decoration and changing it to gold shell coating.

1.2.5 Importance of particle size for magnetic nanoparticles

One of the important difficulties in cancer treatment is that the temperature cannot be distributed evenly throughout the tumor tissue and the tumor starts to grow again as the tumor cells are not completely destroyed. For this reason, ways of targeting directly to tumor cells at the cellular level are being investigated. For this reason, treatment methods that using NPs have been investigated. Particle size is very important in

treatments that using NPs. It is generally between 10-50 nm in applications. Particles of these sizes act as SPIONs, that is, they are in a single magnetic domain and respond faster to AMF application than paramagnetic NPs [29,30]. The size of the coated NPs to be used for hyperthermia treatment should be approximately 30-40 nm. NPs can be modeled either cylindrically or spherically, and between 50-100 nm [96,97].

One of the main factors determining the entry of NPs into the cell or their excretion from the body system is size. For instance, if NPs are smaller than 10 nm, it is rapidly removed from the body through renal clearance, while those larger than 200 nm in diameter are absorbed from the liver and spleen [19].

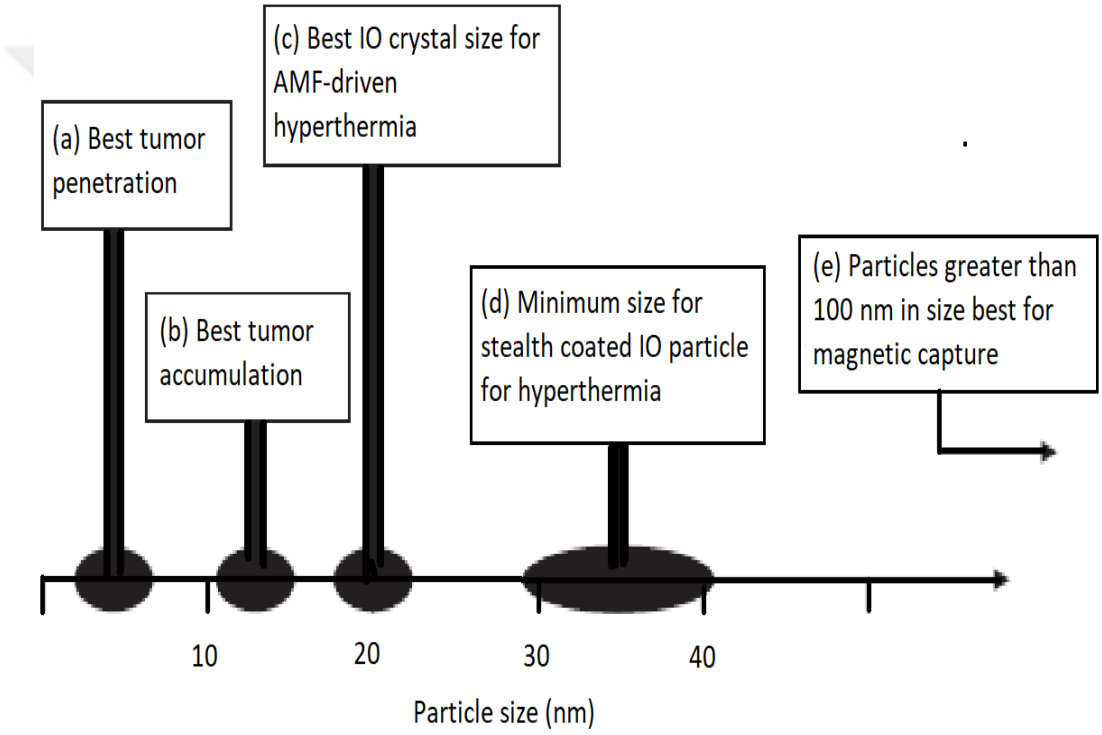

Figure 1.8 **:** Approximative NPs sizes that appear to be most suited for (a) tumor penetration, (b) tumor accumulation, and (c) AMF-Neel relaxation-driven hyperthermia. Also shown are the size ranges for (d) making stealth iron oxide particles for hyperthermia, and (e) particles size needed for magnetic field capture [28].

2. MATERIALS

Purpose of the synthesis of core type NPs, silica coating and amination; $FeCl_2.4H_2O$ **(**Iron (II) chloride tetrahydrate), $FeCl_3.6H_2O$ **(**Iron (III) chloride hexahydrate), $Mg(NO_3)_2.6H_2O$ (Magnesium nitratehedrahydrate(dry)), $Mn(NO_3)_2.4H_2O$ (Manganese (II) nitrate (dry)), NaOH **(**Sodium hydroxide), C_6H_{14} (N-hexane), NH_4OH (Ammonia solution), C_3H_8O (2-propanol) was purchased from Merck (Germany). $Sr(NO3)_2$ (Strontium (II) nitrate (dry)) was purchased from Kimetsan (Turkey). $C_{18}H_{34}O_2$ (oleic acid) was purchased from ZAG (Turkey). De-ionized water produce by evaporation. Evaporator was purchased from Nüve. $C_8H_{20}O_4Si$ (Tetraethyl orthosilicate,TEOS) was purchased from Sigma-Aldrich (Germany). $H_2N(CH_2)_3Si(OCH_3)_3$ (3-aminopropyltrimethoxy-silane) was purchased from Flurochem. (U.K.).

For the purpose of synthesis of gold coating and PEG coating on MNPs; $Na_3C_6H_5O_7$ (Trisodium citrate dihydrate) was used to make gold NPs and supplied from ZAG (Turkey). CH_2O (Formaldehyde,%37) and K_2CO_3 (potassium carbonate) were used in gold-shell coating and purchased from Tekkim (Turkey). PEG-400 (Polyethylene glycol-400) was purchased from ZAG (Turkey) ,it has 380-420 g/mol of molar mass. C_2H_5OH(Ethanol) was supplied from Elif Endüstriyel Kimyasalları (Turkey).

In order to produce $HauCl_4$, Hydrogen chloride (HCl (%37)), HNO_3, was purchased from Merck (Germany) company. Silicone oil was purchased from ZAG (Turkey) company. Pure ingot gold used in order to produce gold chloride (melting process).

Agar was used for gel phantom for magnetic heating experiments, it purchased from ZAG (Turkey).

3. METHODS

3.1 Core Synthesizing

In this study, Fe_3O_4, $MgFe_2O_4$, $MnFe_2O_4$, $SrFe_{12}O_{19}$ MNPs were produced as nuclei and silica coating, amination process, gold coating and PEG coating were performed respectively. Only oleic acid was coated on the core to protect the Fe_3O_4 NPs from oxidation. After calculating the amounts to be used according to the reaction equation given in Figure 3.1 below, the materials are dissolved in distilled water in separate containers and taken into a single container.

Figure 3.1 **:** The solution for core NPs synthesis from left to right respectively : NaOH, $FeCl_3$, $FeCl_2$, $Sr(NO_3)$.

Then the mixer and N_2 gas pipe are placed in the beaker and mixed at 2000 rpm for 30 min. The appropriate amount of NaOH solid is dissolved in distilled water and added to the first mixture. The whole mixture is stirred at 2000 rpm for 3 h. As shown in Figure 3.2, at the end of the process, the mixture is taken on the magnet and the NPs are expected to settle.

Figure 3.2 : Waiting process of NPs on magnet.

Since we grow the NPs in media, the pH (12-13) of the solution is controlled. After the precipitation occurs, the washing process is carried out with the magnet under the beaker. Washing process is continued three times until pH is 7 [98].

The reactions that occurred during the synthesis are given below 3.1, 3.2, 3.3, 3.4:

For Synthesizing Iron Oxide:

$$2FeCl_3.6H_2O + FeCl_2.4H_2O + 8NaOH \rightarrow Fe_3O_4 + 16H_2O + 8NaCl + 2O_2 \quad (3.1)$$

For Synthesizing Strontium Ferrite:

$$2Sr(NO_3)_2 + 8FeCl_2.4H_2O + 16FeCl_3 + 64NaOH \rightarrow 2SrFe_{12}O_{19}\,(s) + 160H_2O + 64NaCl + 3O_2 + 2N_2 \quad (3.2)$$

For Synthesizing Magnesium Ferrite:

$$2Mg(NO_3)_2.6H_2O + 2FeCl_3.6H_2O + 2FeCl_2.4H_2O + 20NaOH \rightarrow 2MgFe_2O_4\,(s) + 42H_2O + 20NaCl + 7O_2 + 2N_2 \quad (3.3)$$

For Synthesizing Manganese Ferrite:

$$4Mn(NO_3)_2.4H_2O + 4FeCl_3.6H_2O + 4FeCl_2.4H_2O + 20NaOH \rightarrow 4MnFe_2O_4\,(s) + 66H_2O + 20NaCl + O_2 + 4N_2 \quad (3.4)$$

3.2 Surface Coating of Superparamagnetic Nanoparticles

3.2.1 Oleic acid coating

The Fe_3O_4 NPs are oxidized since it is known from previous studies that, 0.1 ml of oleic acid was added for each 1g of NPs simultaneously with the addition of NaOH during core synthesis. $MgFe_2O_4$, $MnFe_2O_4$, $SrFe_{12}O_{19}$ NPs are not coated with oleic acid since there is no oxidation problem.

3.2.2 Silica coating and amination of the superparamagnetic nanoparticles

The produced core type NPs are covered with silica using the Stöber method. According to literature researches, TEOS concentration and alcohol type used in silica coating process have an effect on silica coating thickness, structure of NPs and agglomeration of NPs. The TEOS concentration was determined as 25% to obtain the desired silica thickness. First, DI water, solution of NPs and ethanol are mixed at 300 rpm for 30 min. Secondly, ammonia and TEOS are added in appropriate amounts for 20 g of NPs mixture and mixed at 300 rpm for 3 h. After that, it is washed and clarified 5 times with distilled water. In order to amination, APTMS (3-Aminopropyltrimethoxy-silane) is added onto the silica-coated washed NPs and mixed at 300 rpm for 6 h. After that, washing and clarifying processes are done 5 times [98]. Figure 3.3 shows that after washing and clarifying.

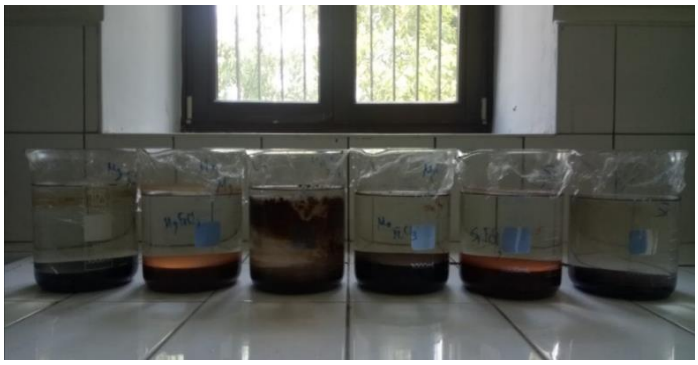

Figure 3.3 : End of the washing and clarifying of the NPs.

3.2.3 Production process for $HAuCl_4$

In the gold chloride production process, there are basically two processes: gold melting and solution purification.

***Melting of gold*:** The beakers must be free from any chemical residue. Cleaning of the beaker is very important as it is a very sensitive reaction. The pure gold bullion weighed is placed into the beaker.

First, HCl is added onto the gold bullion taken into the beaker (no reaction is observed during this time). Then HNO_3 is added dropwise at the rate of 1/4 of HCl. Wait about 5 min for each drop and then another drop was added. Addition of HNO_3 to HCl during addition can cause an explosion when added in the opposite order. When the reaction of the gold ingot is over and the dissolution is over, the ingot that has not melted is weighed again and the process of adding HCl and HNO_3 at a rate of 4 to 1 is continued gradually. Since the boiling of HNO_3 is around 120ºC, adding as little as possible will facilitate purification.

***Purification process*:** For the purification process, 1000 ml of silicone oil was added to a 1500 ml beaker and it was expected to reach 110ºC for about 3 h. After the temperature was kept constant around 110ºC, a small beaker of silicone oil in which the melting process was performed was placed with the help of a hanger. In this setup, the purification was continued at intervals for 2 days. Figure 3.4 shows that purification set up.

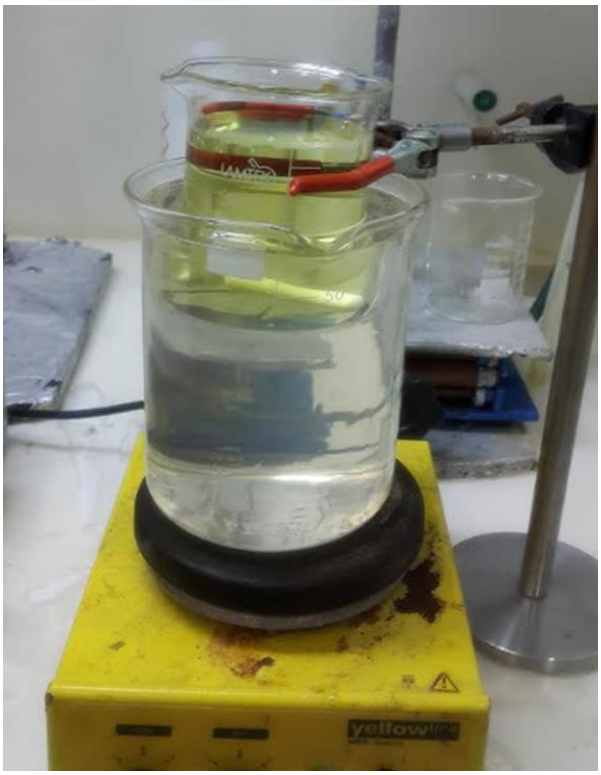

Figure 3.4 : Purification set up for $HauCl_4$ production.

When the beaker dries and a yellowish-orange, after dries the residue must be like slightly wet substance remains at the bottom, Figure 3.5 shown that the residue, pour on distile water and quickly put it in the refrigerator.

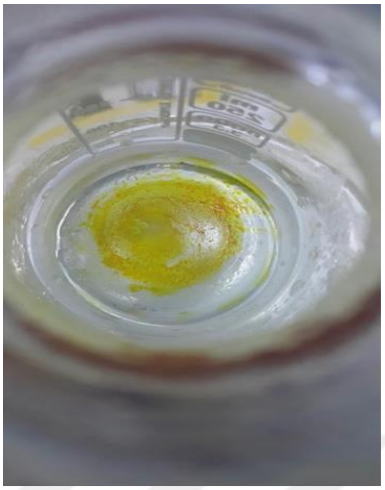

Figure 3.5 **:** The residue on the beaker after purification process.

As shown that Figure 3.6 the color obtained when pouring distile water should be clear yellow.

Figure 3.6 **:** After adding distile water on the residue.

When sodium citrate was added to the sample obtained, it turned wine color, this sample was used for coating.

If the purification process occurs at very high temperatures or for very long periods of time, the orange residue at the bottom dries out completely and turns into pure gold powder. This mean that the process returns to the beginning and this period shows at Figure 3.7. Care should be taken to avoid this.

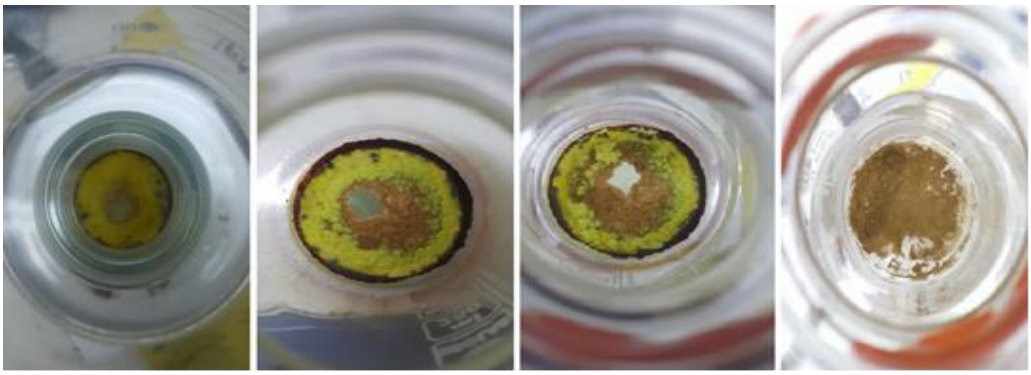

Figure 3.7 **:** All process returns to the beginning and obtain again pure gold powder (right side), if purification temperature more than 110°C.

Temperature monitoring of silicone oil should be measured with a thermo couple every 10 min during boiling and kept constant at 110ºC-115ºC. When the prepared $HAuCl_4$ solution is kept at room temperature, the gold inside metalizes and sinks to the bottom, so it should always be kept in the refrigerator at 4ºC.

3.2.4 Gold coating and gold nanoparticles

Turkevich Method : While 1 mm of 50 ml $HauCl_4$ was boiling, 5 ml of sodium citrate solution of 1% (w/v) was added and stirred with magnetic stirring with no heating via Yellow line MSC Basic C (as shown that Figure 3.9) and as shown that Figure 3.8, $HauCl_4$ turns from pale yellow to transparent color and then to 'red wine colour' in a few min. Boiling is continued for 15 min. When boiling is stopped, it is mixed for 15 min more and the mixture is expected to come to room temperature. Then the mixture is stored in a refrigerator at 4ºC [99].

Figure 3.8 **:** Gold colloidal solution after added 1% (w/v) sodium citrate solution.

First gold NPs coating : We replace the water in 5ml aqueous MNPs by washing it several times with ethanol. We add 50 ml of gold NPs, which we previously added into the centrifuge tube, to 5 ml of ethanol-MNPs, then shake it for a few min. The mixture was left for two hours to settle. Nüve NF 400 Centrifuge Machine used as centrifuge for 10 min at 2000 rpm. The sample is washed 3 times with distilled water. Total volume is made 5 ml as before.

Growing the outer gold layer on the Au coated NPs : Dissolve 25 gr potassium carbonate in 100 ml distilled water and mix for 10 min. While it is mixed, 1.5 ml of aqueous mixture containing 1% $HauCl_4$ is added. When added, the transparent yellow at first begins to become discolored slowly within 30 min. The colour changing that after adding potassium carbonate in 1% $HauCl_4$ was shown in Figure 3.9.

Figure 3.9 : Color change from pale yellow to transparent after added potassium carbonate solution on %1 $HAuCl_4$.

After that, 5 ml of gold-coated MNPs are added on it. Immediately after this step, 0.25 ml formaldehyde is added quickly. Centrifuge and rinse with distilled water several times. The total volume is 5ml as in the baseline [100].

3.2.5 PEG coating

For 5 ml Au coated MNPs 1.5 ml PEG400 is added at room temperature and mixed for 15 min. It is then incubated for 12 h at room temperature. The mixture is centrifuged at 4100 rpm for 20 min, the supernatant is rinsed with distilled water and added to 10 ml again [101].

3.3 Characterisation Techniques of Magnetic Nanoparticles

3.3.1 Scanning electron microscopy (SEM)

Surface morphology of MNPs samples were analyzed by SEM (Tescan VEGA3) in Istanbul Technical University TEMAG Laboratory. Quantitative chemical characterization of the produced filters was made by Energy Dispersive X-ray Spectroscopy (EDX). EDX is a technique for analyzing characteristic X-rays generated from the electron beam-sample interaction to provide the basic composition of the sample in the form of spectra. Each peak in the EDX spectrum corresponds to characteristic X-ray lines of the particular element. Thus, spectra provide quantitative chemical characterization of samples.

3.3.2 Fourier transform infrared spectroscopy (FTIR)

The principle of Fourier transform infrared spectroscopy is based on the specific absorption of electromagnetic waves of chemical groups such as amine, carboxyl groups or hydroxyl groups. It was analyzed whether the synthesized nanoparticles have characteristic bonds by performing FTIR analysis. Bruker optics ALPHA-Transmittance FTIR spectrometer was used. 1 g of NP in 30 g solution, 30 ml of NPs solution was prepared and dried in Alex Machine Ultrasonic Water Bath at 80ºC-85ºC for 12 hours. The samples were then beaten in a mortar and pulverized for FTIR analysis.

3.4 Heating Experiments Of Superparamagnetic Nanoparticles

3.4.1 Adjusting of nanoparticles for heating experiment

In the comparison experiments of SPIONs, the ratio of 0.1% (v/m) (volume of nanoparticle liquid ml / mg of total liquid in the heating vessel) was used as the ratio.

The formula d=m/v was used to prepare the magnetic fluid containing NPs according to this ratio. The density of $SrFe_{12}O_{19}$, $MnFe_2O_4$, Fe_3O_4 and $MgFe_2O_4$ NPs was taken as 5.3 mg/ml, 5.3 mg/ml, 5 mg/ml, 4.7 mg/ml, respectively. The density of water is taken as 1000 mg/ml.

The vessel that we used for heating experiments takes a total of 2000 mg of distilled water. According to the ratio that we determined as 0.1% (v/m), there should be

milligrams of NPs equivalent to 2 ml of NPs liquid in our test vessel. According to d=m/v calculation; This means that there is 10.6 mg of NPs for $MnFe_2O_4$ and $SrFe_{12}O_{19}$, 10 mg for Fe_3O_4, 9.4 mg for $MgFe_2O_4$ in a heating vessel containing 2000 mg of distilled water.

The NP liquids were taken from the main vessel with a pipette in 1 ml of NPs liquid as 10.6 mg, 10.6 mg, 10 mg and 9.4 mg of NPs for $SrFe_{12}O_{19}$, $MnFe_2O_4$, Fe_3O_4, and $MgFe_2O_4$, respectively, and added to the heating vessel. Then, 1 ml of agar gel (prepared with distilled water) was added on it if it was to be heated in agar phantom. If it is to be heated in water media, 1 ml of distilled water is added on it.

3.4.2 Preparation of NP/agarose samples

The amount of agar powder was calculated as 1% of distilled water. First, 10 ml of distilled water was added to the beaker, then 2 ml of distilled water was added and heated with a heater (the reason for adding an extra 2 ml of water is to compensate for the loss of evaporation when the solution is heated). When the water temperature is 50°C, 0.1 mg powder agar is added to the water and mixed using magnetic fish. Heating of the solution continues until small bubbles are formed in the solution. This process continues for about 10 min and is mixed at high speed.After the bubbles formed, the beaker was taken from the heater and stirred on the cold mixer until the temperature dropped to 70°C. Then, 1 ml of solution was pipetted and added to the MNPs solution. Mixing was continued with a small mixing device until the solution hardened. Figure 3.10 shows that preparation of agarose/NPs mixture.

Figure 3.10 : Preparation of agarose/NPs mixture.

After the agar has cooled and hardened (Figure 3.11), the glass agar vessel were placed on the helical coil in the induction generator and its heating performance under AMF was examined.

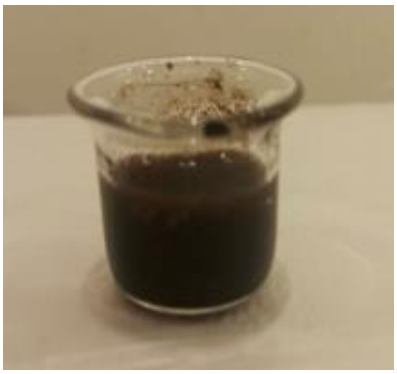

Figure 3.11 : NPs/agarose sample in the glass vessel after agarose gel became hardened.

In the heating experiments the process of heating the NPs in distile water using a helical coil was carried out.

3.4.3 Heating experiment set up

The experimental setup; An induction generator was used to heat the MNPs. Power between 0-5 kW can be supplied with an alternating induction generator and different coils can be used. Helical coil was used in the study.

The samples were subjected to the heating experiment under AMF. In the experiments, the surface temperature of the sample was measured at intervals of 1 sec with the Optris CF-4 laser thermometer. Figure 3.12 shows that the Optris CF-4 laser thermometer.

Figure 3.12 : Optris CF-4 laser thermometer

These measurements were recorded with the help of the Compact Connect program, as shown in the Figure 3.13, in order to draw the heating-time graph of the materials.

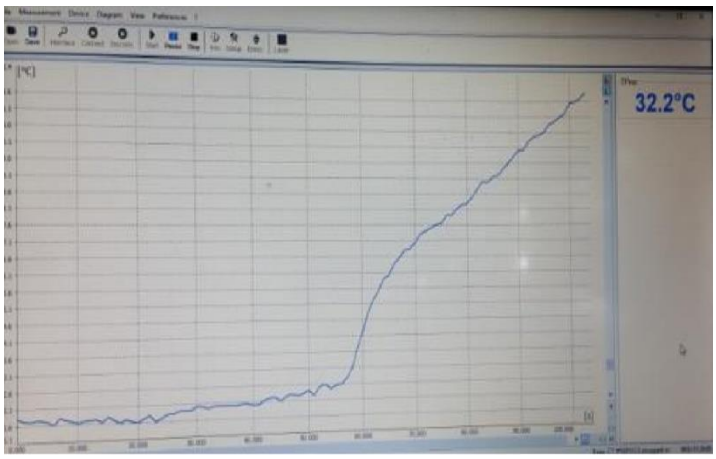

Figure 3.13 : Receiving heating data with the Compact Connect Program.

In order to control the magnetic power given during the experiments, the variable current data in the coil was taken with the help of a helical coil and a Transducer (PEM), and these data were read through Oscilloscope (ADS 3072B-70 MHz-1GSa/s). Transducer and Osciloscope are given in Figure 3.14 and Figure 3.15 respectively.

Figure 3.14 : Transducer.

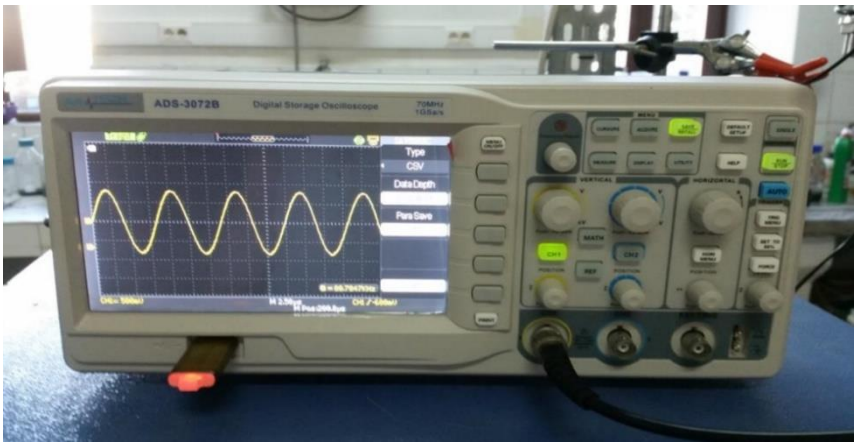

Figure 3.15 : Osciloscope.

Helical coil was used in the experimental setup. The helical coil given in Figure 3.16 and Figure 3.17.

Figure 3.16 : Geometry of the helical coil that used in heating experiments.

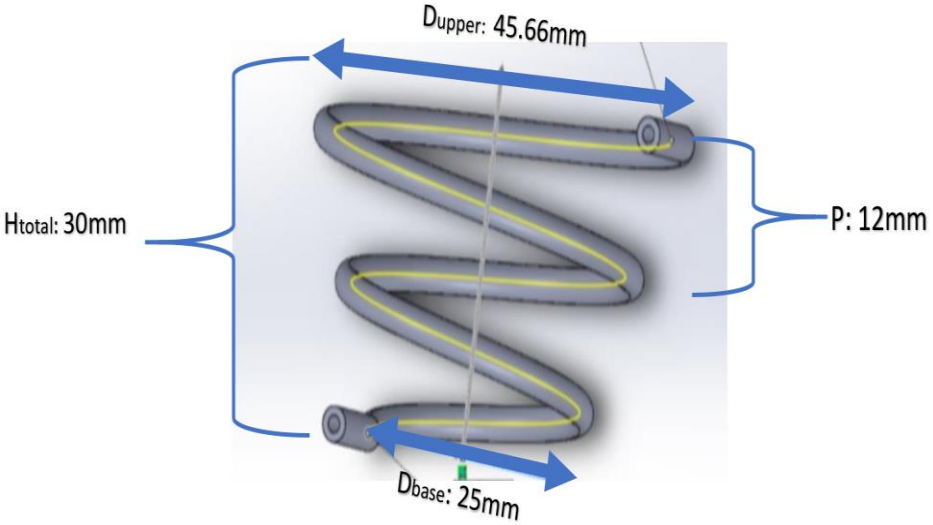

Figure 3.17 : Dimensions of helical coil.

SAYKON Enerji induction generator was used and its specifitions given in Table 3.1. All equipment in heating experimental set up given in Figure 3.18.

Figure 3.18 : Heating experimental set up with whole equipments: (1) Computer with Compact Connect Programme, (2) laser thermometer, (3) oscilloscope, (4) thermal camera, (5) PLC for laser thermometer, (6) thermometer, (7) black box for magnetic field and (8) induction generator.

Table 3.1 : Specifications of induction generator.

Parameters	Value
Maximum power output	5 [kW]
Current intensity	300 [A]
Operation frequency	132 [kHz]
Heigh of each helical (P)	12mm
Coil turns	2,5
Ground clearance (H_{total})	30mm
Diameter of coil base (D_{base})	25mm
Diameter of coil upper (D_{upper})	45.66mm

4. RESULTS AND DISCUSSION

4.1 Characterization Of Superparamagnetic Nanoparticles

The FTIR spectrum was used to determine the core NPs, silica coating, amination, gold coating, and PEG coatings. In Table 4.2, there are specific vibration peaks similar to fingerprints for each material, using them the structure of each material is determined by FTIR. Table 4.1 shows that the list of materials abbreviation. Fe_3O_4 NPs are oxidized since it is known from previous studies that, 0.1 ml of oleic acid was added for each 1g of NPs simultaneously with the addition of NaOH during core synthesis. $MgFe_2O_4$, $MnFe_2O_4$, $SrFe_{12}O_{19}$ NPs are not coated with oleic acid since there is no oxidation problem.

Table 4.1 : The list of materials abbreviation.

Material	Core (C)	Silica on C	Aminated on SC	Gold on ASC	PEG on GASC
Fe_3O_4	Fe_C	Fe_SC	Fe_ASC	Fe_GASC	Fe_PGASC
$MnFe_2O_4$	Mn_C	Mn_SC	Mn_ASC	Mn_GASC	Mn_PGASC
$MgFe_2O_4$	Mg_C	Mg_SC	Mg_ASC	Mg_GASC	Mg_PGASC
$SrFe_{12}O_{19}$	Sr_C	Sr_SC	Sr_ASC	Sr_GASC	Sr_PGASC

Table 4.2 : FTIR bands in literature.

Chemical bond	Characteristic vibration band [cm^{-1}]	Literature source
Fe3O4 NPs		
Fe-O	563,540,581,586	[53], [102], [103], [104]
Fe-O-Fe	568	[105]
SrFe12O19 NPs		
Sr-O	524, 625	[105]
Sr-Fe	400-600	[106]
MgFe2O4 NPs		
Mg-O	1016, 1627	[108], [109]
Mg-Fe	582, 473,697, 560	[107], [108], [109]
MnFe2O4 NPs		
Mn-O	1382, 1458, 1638	[109]
Mn-Fe	697, 700-1100	[109], [110]
Mn-OH	1641, 1428, 1237	

Table 4.2 (continued) : FTIR bands in literature.

Chemical bond	Characteristic vibration band [cm-^{1}]	Literature source
Oleic acid coating on Fe_3O_4_Core NPs		
Fe-COO	1398, 1628	[53]
	1541, 1639, 1438	[111], [112]
H-C-H	2922, 2852	[111], [112]
C-O	1050	[111], [112]
Silica coating		
Fe-O-Si	524, 625	[105]
Si-O	400-600	[103], [104]
Si-O-Si		[53]
SiO4		[103]
Hydroxil groups		
O-H	1630, 3400	[103] [104]
	3500-3200	[113]
	3500-3200	
Amin groups		
N-H	1382, 1458, 1638	[113]
	697, 700-1100	[113] [114]
	1641, 1428, 1237	[114]
PEG coating		
-CH_2 stretching	2850-3000	[115], [116], [117]
N-H bending	1631	
C=O stretching	1660	
C-H bending -CH_2, -CH_3	1380	
C-O-C stretching	1100	
N-H wagging	600-900	

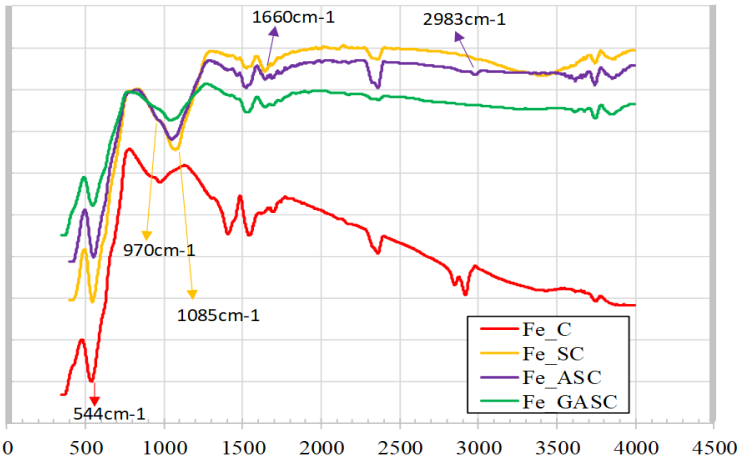

Figure 4.1 : FTIR spectra for Fe_C, Fe_SC, Fe_ASC, Fe_GASC (Fe_PGASC is omitted).

Figure 4.1 shows the vibration bands of Fe_3O_4. Vibration bands (Fe-O, Fe-O-Fe) for Fe_3O_4, vibration range is 500-650 cm^{-1}. The vibration at 544 cm^{-1} in our example indicates the presence of Fe-O, Fe-O-Fe. The IR band at 1085 cm^{-1}, which consists of the presence of Si-O, Si-O-Si, indicates the presence of silica coating. IR bands at 1660 cm^{-1} and 2983 cm^{-1} are due to the presence of N-H primary bonds, which indicates that the amination process has been performed. FTIR result could not be obtained for the PEG coated Fe_3O_4.

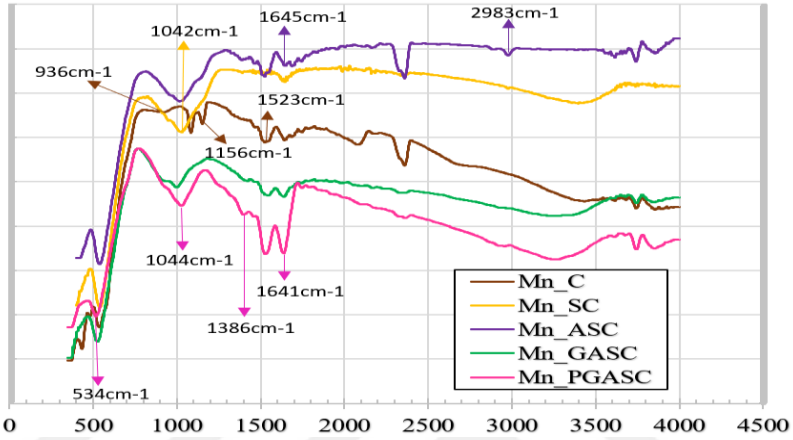

Figure 4.2: FTIR spectra for Mn_C, Mn_SC, Mn_ASC, Mn_GASC and Mn_PGASC

Figure 4.2 shows the vibration bands of Mn-O, Mn-Fe, Mn-OH bonds found in $MnFe_2O_4$ NPs, the IR bands at 523-936-1156 cm^{-1} and 1656 cm^{-1} in FTIR results indicate the presence of these bonds and $MnFe_2O_4$ NPs. IR bands at 1042 cm^{-1} and 952 cm^{-1}, which are formed by the presence of Si-O and Si-O-Si, indicate the presence of silica coating. IR bands at 1645 cm^{-1} and 2983 cm^{-1} are due to the presence of N-H primary bonds, which indicates the presence of amination.

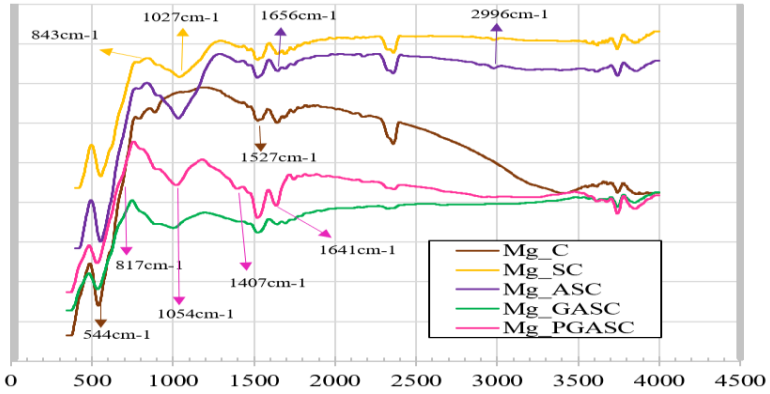

Figure 4.3 : FTIR spectra for Mg_C, Mg _SC, Mg _ASC, Mg _GASC and Mg_PGASC.

Figure 4.3 shows the vibration bands of $MgFe_2O_4$. The Mg-O vibration bands must be at 1016 cm^{-1} and 1627 cm^{-1} and Mg-Fe vibration bands must be at 473-560-582-697 cm^{-1}, the IR vibration bands at 1527 cm^{-1} and 544 cm^{-1} shown in the graph prove the presence of these bonds and the presence of the $MgFe_2O_4$ NPs. The IR band at 1027 cm^{-1}, which consists of the presence of Si-O and Si-O-Si, indicates the presence of silica coating. IR bands at 1656 cm^{-1} and 2996 cm^{-1} are due to the presence of N-H primary bonds, which indicates the presence of amination.

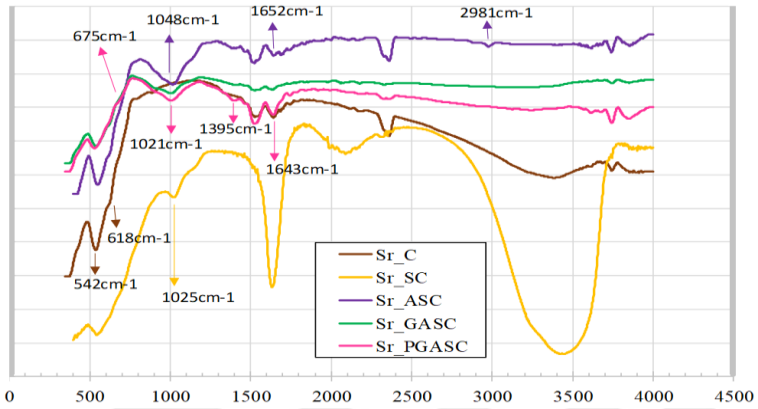

Figure 4.4 **:** FTIR spectra for Sr_C, Sr _SC, Sr _ASC, Sr _GASC and Sr _PGASC

Sr-Fe vibration bands must be at between 400-600 cm^{-1} and Sr-O vibration bands between 524-625 cm^{-1}. The 542 cm-1 and 618 cm^{-1} vibrations shown in Figure 4.4, prove the existence of these bonds and the existence of the $SrFe_{12}O_{19}$ NPs. The IR band at 1025 cm^{-1}, which consists of the presence of Si-O and Si-O-Si, indicates the presence of silica coating. IR bands at 1652 cm^{-1} and 2981 cm^{-1} indicate the presence of amination due to the presence of N-H primary bonds.

For approve gold shell , there must be reducing of the intensity of Si-O-Si and Si-OH peaks.

Vibration bands proving the existence of PEG define as follows: 2850-3000 cm^{-1} (-CH2 stretching), 1631 cm^{-1} (N-H bending), 1660 cm^{-1} (C=O stretching), 1380 cm^{-1} (C-H bending; $-CH_2$ and $-CH_3$), 1100 cm^{-1} (C-O-C stretching) and 600-900 cm^{-1} (N-H wagging). These vibration bands supported the surface functionalization of the MNPs was successful and approve the presence of bound PEG.

Table 4.3 : SEM results.

Material	Core (C) Diameter	SC Diameter	GASC Diameter
Fe_3O_4	19.50	21.66	24.32
$MnFe_2O_4$	21.07	22.55	26.88
$MgFe_2O_4$	21.93	22.62	24.24
$SrFe_{12}O_{19}$	21.60	17.98	23.08

According to the results of SEM analysis, the coating thickness has gradually increased from core to gold coating. Table 4.3 shows that SEM result. Only the thickness of the silica coated $SrFe_{12}O_{19}$ sample was lower than the core sample. Samples could not be selected clearly due to astigmatic problems in SEM measurements. For trusty morfology results must be use TEM measurement.

4.2 The Results Of Magnetic Heating Experiments

The heating performances of MNPs with 5 different coating layers and 4 different nuclei produced for the hyperthermia cancer therapy protocol were compared.

In the study , NPs were prepared in two different media as agar phantom and water media and subjected to heating test. Agar phantom has been used as it resembles the heating pattern of human tissue. At the same time, since the agar phantom has a gel consistency, the NPs did not settle to the bottom and a homogeneous distribution was achieved. Tests conducted in the water media were made to be compared with the heating tests found in the literature. However, a homogeneous mixture cannot be obtained in the heating tests performed in water media as in the agar phantom. In the experiments, the maximum power of the machine, 5kw, was used in order to provide heating in a short time.

In the first stage of the experiments, it was aimed to determine the 'SPIONs type' with the best heating capacity among 4 different SPIONs types. For this purpose, 4 different core SPIONs were subjected to heating experiments in water environment (Figure 4.5) and then in agar phantom (Figure 4.6). As a summary table of these two figures is given in Table 4.4 for better understanding. According to Table 4.4, Mg SPIONs determined as the fastest heating performance SPIONs.

Table 4.4 : The seconds given in the table is the time that the sample reaches 42°C.The summary table of Figure 4.5 and Figure 4.6

Material	First reach	Second reach	Third reach	Fourth reach
In water media	Mg_C (145 sec)	Mn_C (146 sec)	Fe_C (171 sec)	Sr_C (222 sec)
In agar phantom	Mg_C (187 sec)	Mn _C (196 sec)	Fe _C (249 sec)	Sr_C (293 sec)

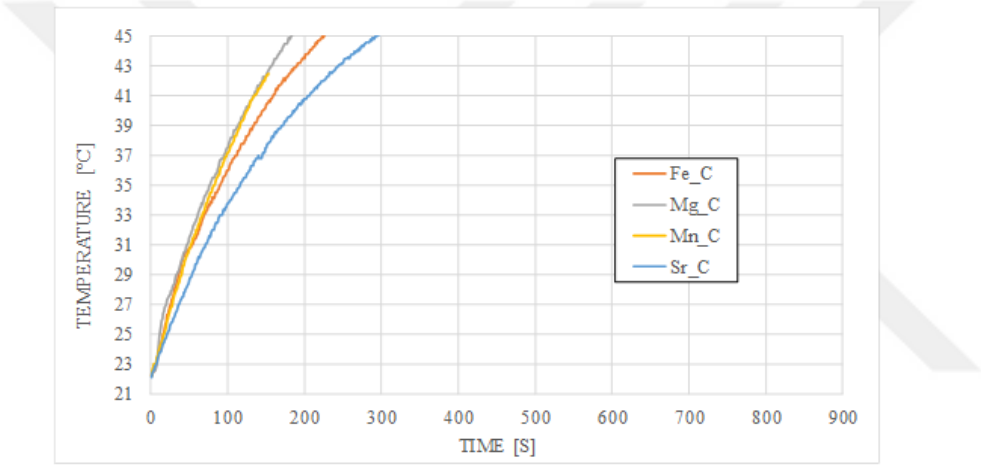

Figure 4.5 **:** Heating curves of Fe_C, Mg_C, Mn_C, Sr_C in water media as % 0.1 (v/v) equal volume ratio at 5 kw.

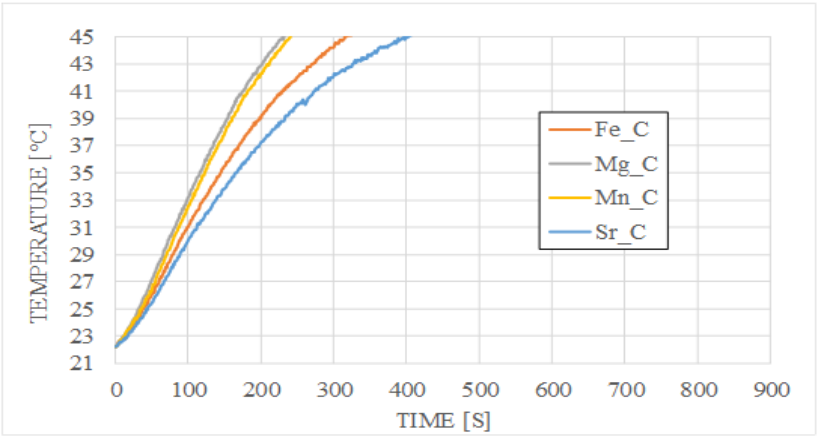

Figure 4.6 **:** Heating curves of Fe_C, Mg_C, Mn_C, Sr_C in agar phantom as % 0.1 (v/v) equal volume ratio at 5 kw.

In the second stage, our purpose was to 'determine the amount' we could reach 42°C in the shortest time by using the lowest amount of NPs possible. For this purpose, '$MgFe_2O_4$ core SPIONs', which have the fastest heating performance, were firstly tested at 5 different concentrations, 1mg/ml, 2.5 mg/ml, 5 mg/ml, 7.5 mg/ml, 10 mg/ml, 'in the water media' (Figure 4.7). As a result of the experiment, the lowest concentration (1 mg/ml) couldn't reach 42°C, because of this reason, this concentration didn't used in other experiments.

Afterwards, in the same process like 'second stage', heating experiments at other 4 concentrations, 2.5 mg/ml, 5 mg/ml, 7.5 mg/ml, 10 mg/ml, were performed (Figure 4.8) without using 1mg/ml 'in agar phantom'. The sample prepared at a concentration of 2.5 mg/ml showed the lowest heating performance. Therefore, this concentration didn't used in other experiments. Concentrations of 7.5 mg/ml and 10 mg/ml didn't used in other heating experiments, since the aim of the treatment was to enject the lowest possible NPs dosage for to the patient. As a summary table of these 2 figures is given in Table 4.5 for better understanding.

Table 4.5 : The seconds given in the table is the time that the sample reaches 42°C.The summary table of Figure 4.7 and Figure 4.8

Material	1 mg/ml	2.5 mg/ml	5 mg/ml	7.5 mg/ml	10 mg/ml
Mg_C (water)	X	394 sec	188 sec	142 sec	77 sec
Mg_C (agar)	-	381 sec	194 sec	143 sec	112 sec

According to Table 4.5, it was determined that the NPs at the lowest dosage was 5mg/ml with the highest heating performance, and this concentration was maintained in our other heating experiments.

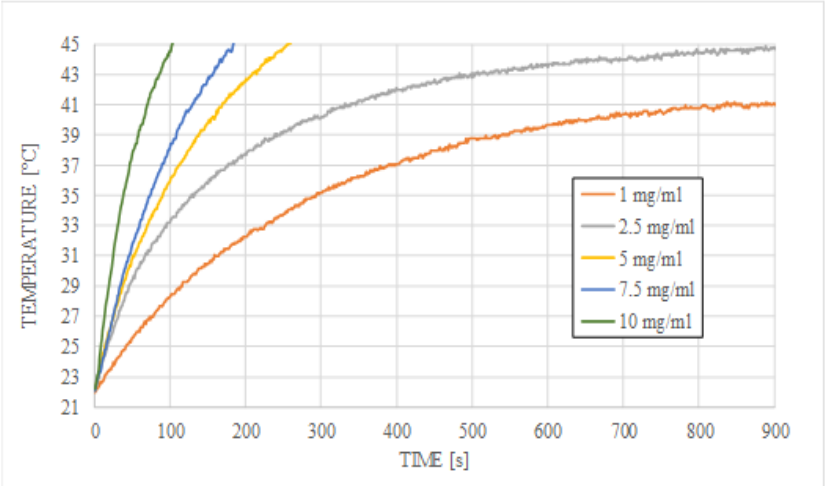

Figure 4.7 **:** Heating curves of Mg_C with different concentration in water at 5 kw.

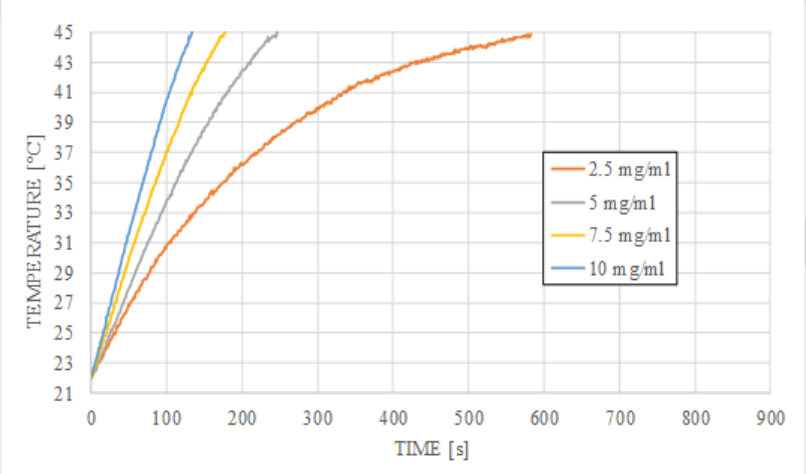

Figure 4.8 **:** Heating curves of Mg_C with different concentration in agar phantom at 5 kw.

In the third stage, the heating performance of '4 different SPIONs varieties' were compared with each other 'in agar phantom'. Figure 4.6, Figure 4.9, Figure 4.10, Figure 4.11 and Figure 4.12 show the comparison of 4 different SPIONs in the core, silica coating, amination, gold coating and PEG coating stages, respectively. As a summary table of these 5 Figures is given in Table 4.6 for better understanding. According to the table 4.6, $MgFe_2O_4$-SPIONs gave the fastest performance in all layer types except PEG coated. The lowest performance was given by $SrFe_{12}O_{19}$-SPIONs in all layer types.

Table 4.6 : The sequence of 'surface coating steps' when the samples reaching at 42°C in agar phantom. The seconds given in the table is the time that the sample reaches 42°C. This table summary about Figure 4.6 and Figure 4.9, Figure 4.10, Figure 4.11 and Figure 4.12.

Surface coating steps	First reach	Second reach	Third reach	Fourth reach
Core	Mg_SC (187 sec)	Mn_SC (196 sec)	Fe_SC (249 sec)	Sr_SC (293 sec)
Silica coating	Mg_SC (171 sec)	Mn_SC (172 sec)	Fe_SC (245 sec)	Sr_SC (395 sec)
Amination	Mg_ASC (150 sec)	Mn_ASC (186 sec)	Fe_ASC (245 sec)	Sr_ASC (379 sec)
Gold coating	Mg_GASC (196 sec)	Mn_GASC (201 sec)	Fe_GASC (216 sec)	Sr_GASC (251 sec)
PEG coating	Mn_PGASC (187 sec)	Mg_PGASC (211 sec)	Fe_PGASC (243 sec)	Sr_PGASC (372 sec)

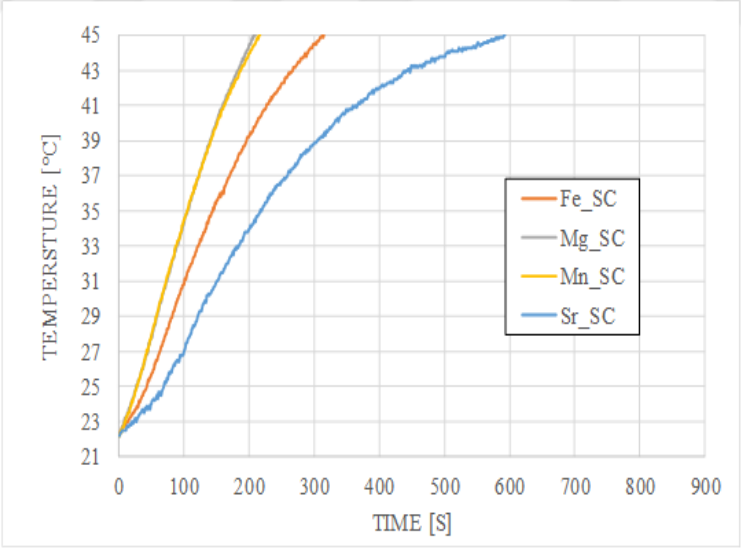

Figure 4.9 **:** Heating curves of Fe_SC, Mg_SC, Mn_SC, Sr_SC in agar phantom as % 0.1 (v/m) equal ratio at 5 kw.

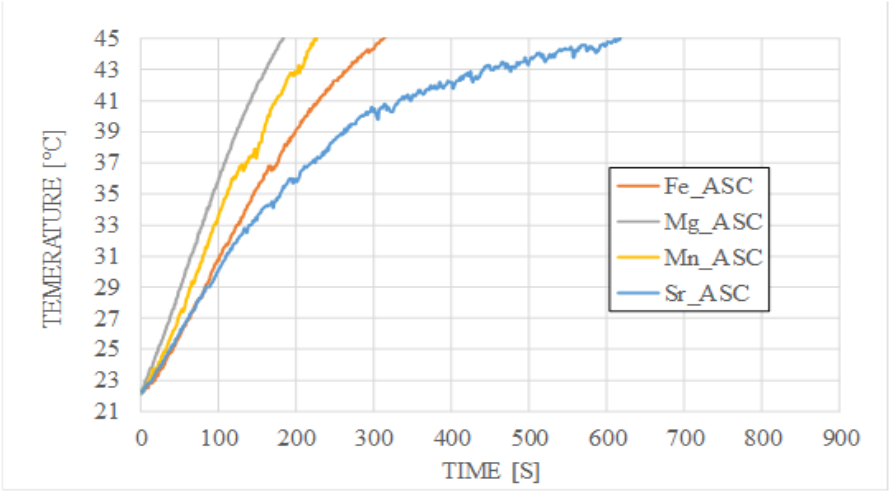

Figure 4.10 **:** Heating curves of Fe_ASC, Mg_ASC, Mn_ASC, Sr_ASC in agar phantom as % 0.1 (v/m) equal ratio at 5 kW.

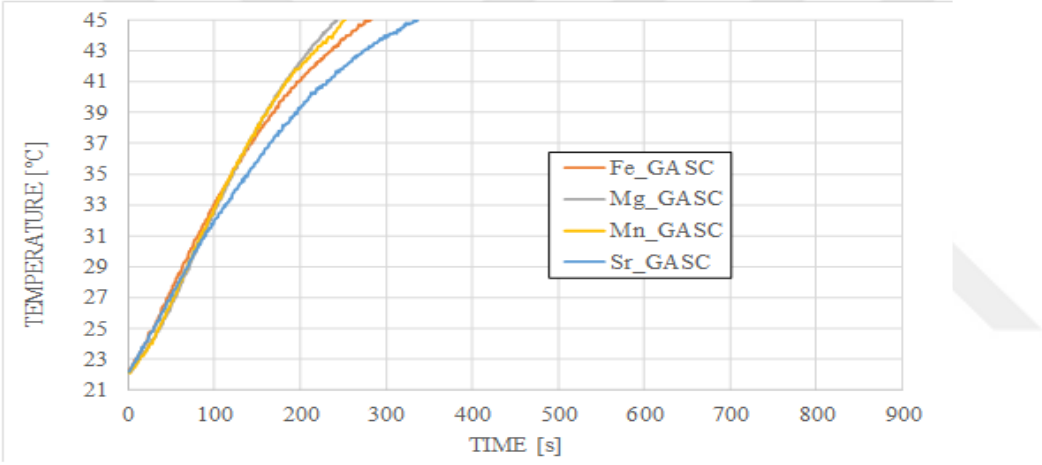

Figure 4.11 **:** Heating curves of Fe_GASC, Mg_GASC, Mn_GASC, Sr_GASC in agar phantom as % 0.1 (v/m) equal ratio at 5 kW.

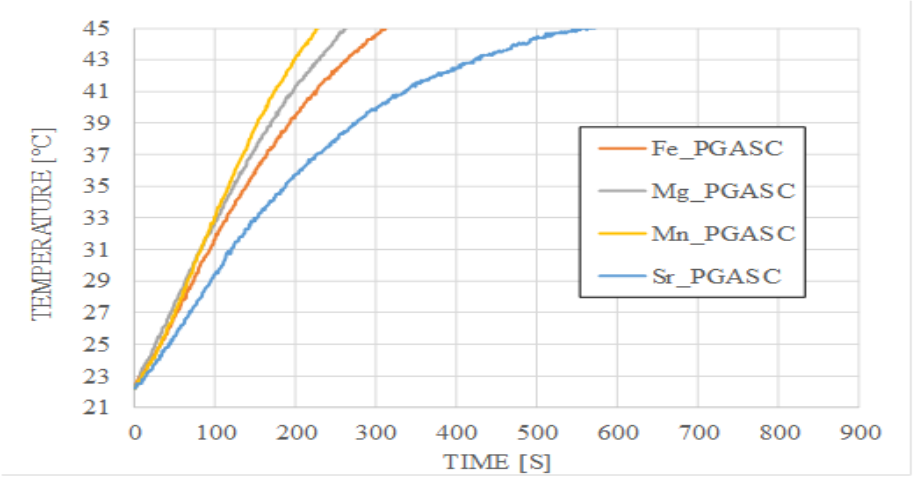

Figure 4.12 **:** Heating curves of Fe_PGASC, Mg_PGASC, Mn_PGASC, Sr_PGASC in agar phantom as % 0.1 (v/m) equal ratio at 5 kW.

In the fourth stage, the same comparison (third stage comparison) was made 'in water media'. Figure 4.13, Figure 4.14, Figure 4.15, Figure 4.16 and Figure 4.17 show the comparison of SPIONs in core, silica coating, amination, gold coating and PEG coating stages, respectively. A summary table of these 5 figures is given in Table 4.7 for better understanding. According to the Table 4.7, $MgFe_2O_4$-SPIONs gave the fastest performance in all layer types.

Table 4.7 : The sequence of 'surface coating stages' when the samples reaching at 42°C in water media. The seconds given in the table is the time that the sample reaches 42°C. This table about between Figure 4.13 and Figure 4.17.

Surface coating steps	First reach	Second reach	Third reach	Fourth reach
Core	Mg_SC (145 sec)	Mn_SC (146 sec)	Fe_SC (171 sec)	Sr_SC (222 sec)
Silica coating	Mg_SC (130 sec)	Mn_SC (145 sec)	Fe_SC (173 sec)	Sr_SC (233 sec)
Amination	Mg_ASC (124 sec)	Mn_ASC (139 sec)	Fe_ASC (179 sec)	Sr_ASC (209 sec)
Gold coating	Mg_GASC (146 sec)	Mn_GASC (153 sec)	Fe_GASC (176 sec)	Sr_GASC (249 sec)
PEG coating	Mg_PGASC (150 sec)	Mn_PGASC (165 sec)	Fe_PGASC (231 sec)	Sr_PGASC (279 sec)

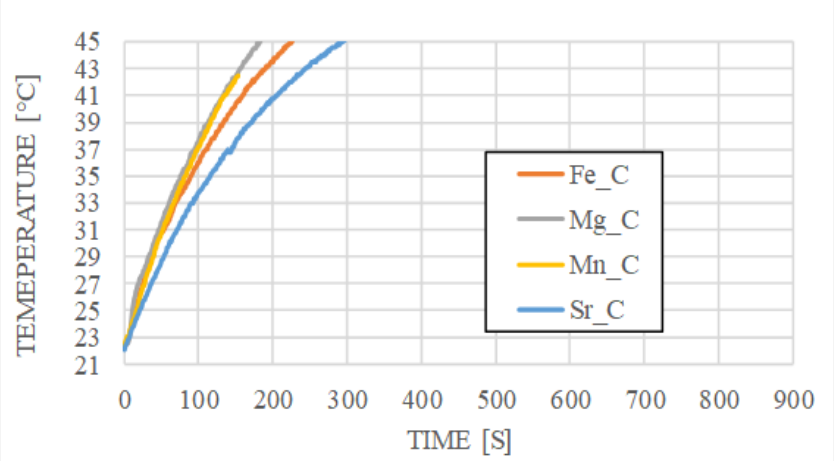

Figure 4.13 : Heating curves of Fe_C, Mg_C, Mn_C, Sr_C in water media as % 0.1 (v/m) equal ratio at 5 kW.

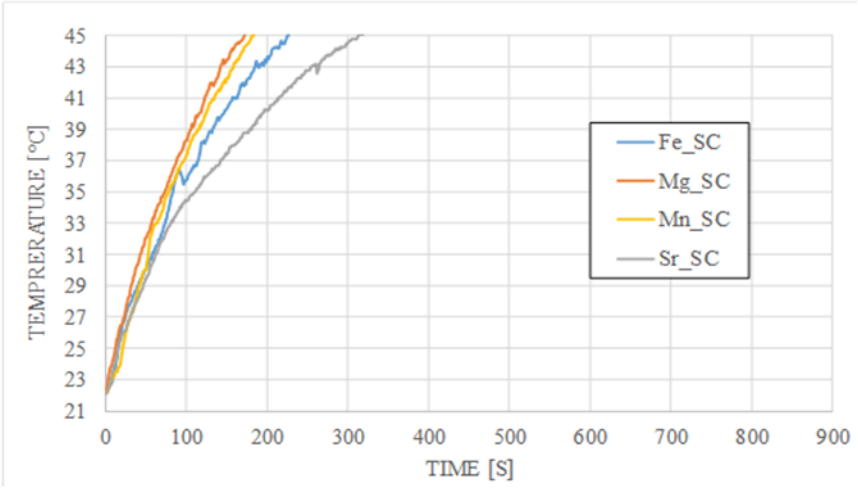

Figure 4.14 **:** Heating curves of Fe_SC, Mg_SC, Mn_SC, Sr_SC in water media as % 0.1 (v/m) equal ratio at 5 kW.

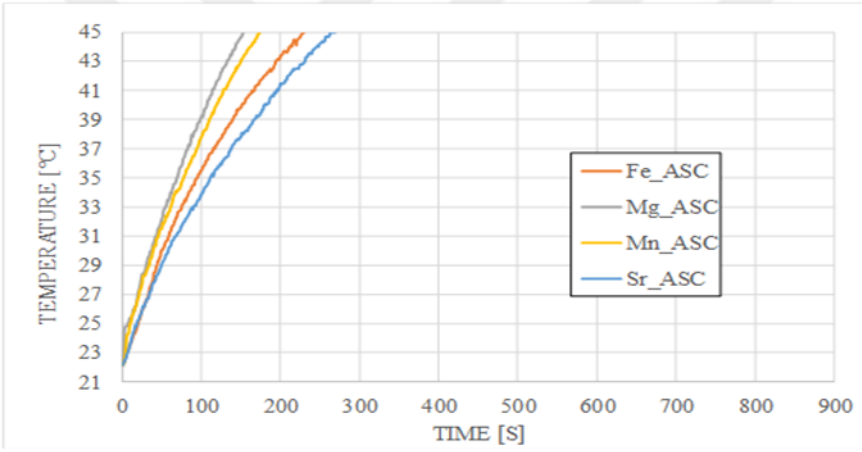

Figure 4.15 **:** Heating curves of Fe_ASC, Mg_ASC, Mn_ASC, Sr_ASC in water media as % 0.1 (v/m) equal ratio at 5 kW.

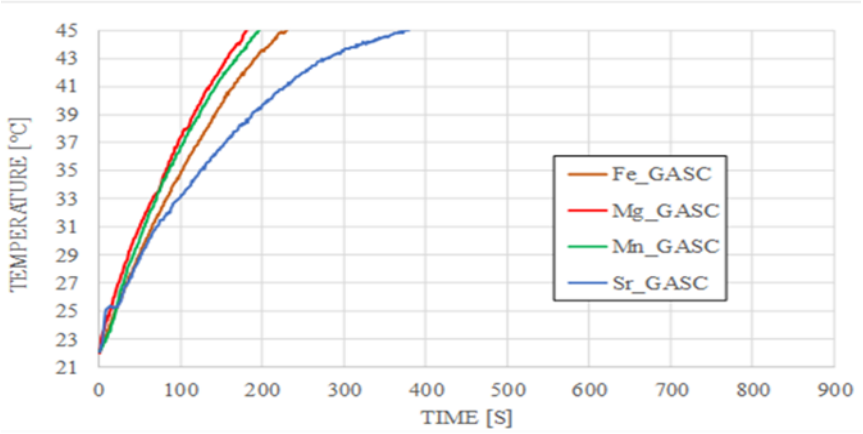

Figure 4.16 **:** Heating curves of Fe_GASC, Mg_GASC, Mn_GASC, Sr_GASC in water media as % 0.1 (v/m) equal ratio at 5 kW.

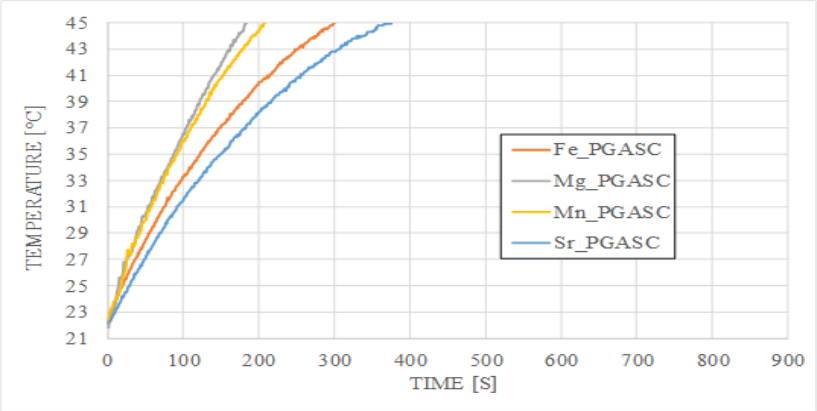

Figure 4.17 : Heating curves of Fe_PGASC, Mg_PGASC, Mn_PGASC, Sr_PGASC in water media as % 0.1 (v/m) equal ratio at 5 kW.

In the fifth and last stage, the heating performance of '5 different coating types' was compared 'in the water media'. Figure 4.18, Figure 4.19, Figure 4.20 and Figure 4.21 show the comparison of the heating performance of Fe_3O_4, $MnFe_2O_4$, $MgFe_2O_4$ and $SrFe_{12}O_{19}$ SPIONs at different layer stages, respectively. A summary table of these 4 figures is given in Table 4.8 for better understanding. According to the Table 4.6, amination SPIONs gave best heating performance in all types SPIONs except Fe_3O_4-SPIONs. In all SPIONs types, PEG coated SPIONs gave the lowest heating performance. In all SPIONs types except Fe_3O_4-SPIONs, gold coated SPIONs gave the lowest heating performance after PEG coated SPIONs.

Table 4. 8 : The sequence of 'SPIONs type' when the samples reaching at 42°C in water media. The seconds given in the table is the time that the sample reaches 42°C. This table about between Figure 4.18 and Figure 4.21.

Material	First reach	Second reach	Third reach	Fourth reach	Fifth reach
Fe3O4	Fe_C (171 sec)	Fe_SC (173 sec)	Fe_GASC (176 sec)	Fe_ASC (179 sec)	Fe_PGASC (231 sec)
$MnFe_2O_4$	Mn_ASC (139 sec)	Mn_SC (145 sec)	Mn_C (146 sec)	Mn_GASC (153 sec)	Mn_PGASC (165 sec)
$MgFe_2O_4$	Mg_ASC (124 sec)	Mg_SC (130 sec)	Mg_C (145 sec)	Mg_GASC (146 sec)	Mg_PGASC (150 sec)
$SrFe_{12}O_{19}$	Sr_ASC (209 sec)	Sr_SC (222 sec)	Sr_C (233 sec)	Sr_GASC (249 sec)	Sr_PGASC (279 sec)

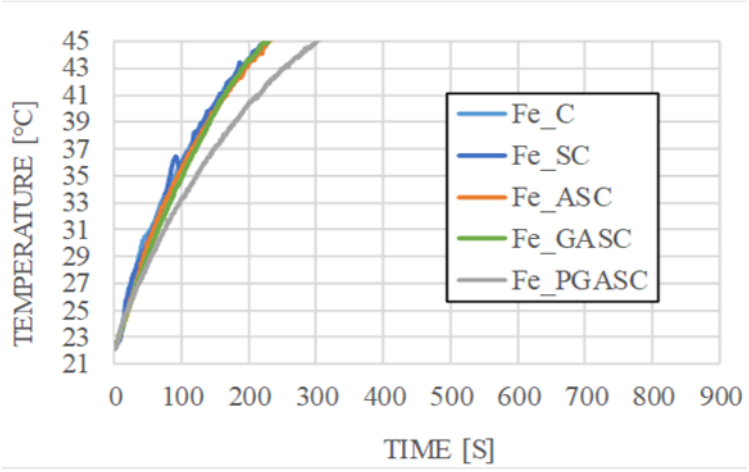

Figure 4.18 **:** Heating curves of Fe_C, Fe _SC, Fe _ASC, Fe _GASC, Fe _PGASC in water media as % 0.1 (v/m) equal ratio at 5 kW.

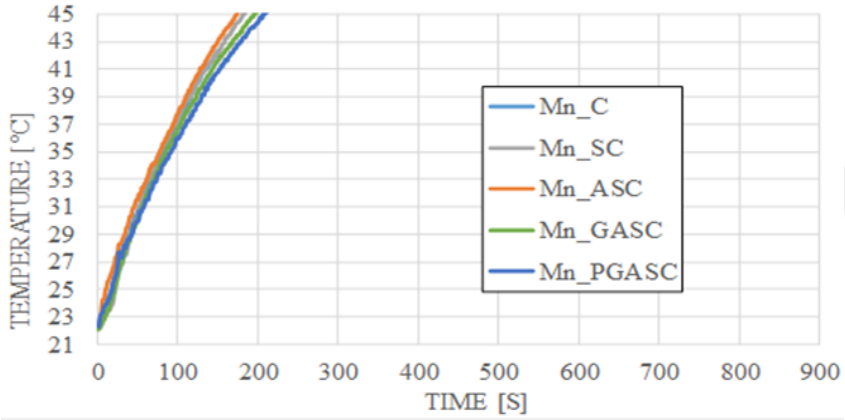

Figure 4.19 **:** Heating curves of Mn_C, Mn_SC, Mn_ASC, Mn_GASC, Mn_PGASC in water media as % 0.1 (v/m) equal ratio at 5 kW.

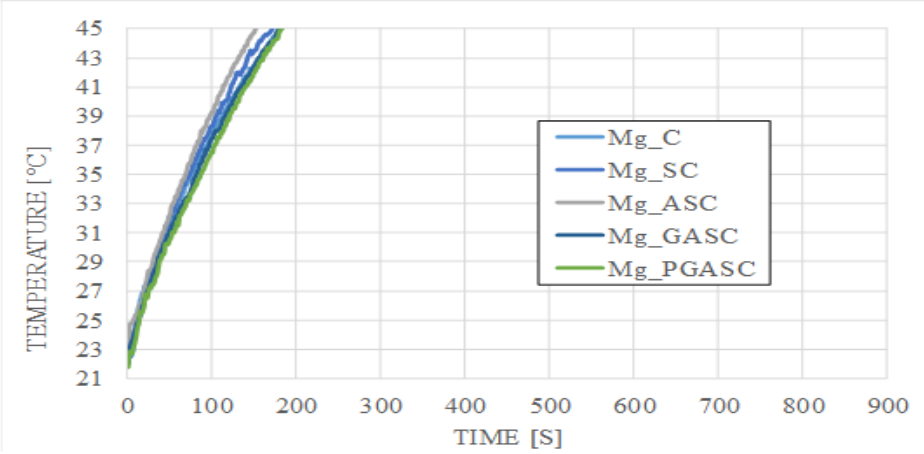

Figure 4.20 **:** Heating curves of Mg_C, Mg_SC, Mg_ASC, Mg_GASC, Mg_PGASC in water media as % 0.1 (v/m) equal ratio at 5 kW.

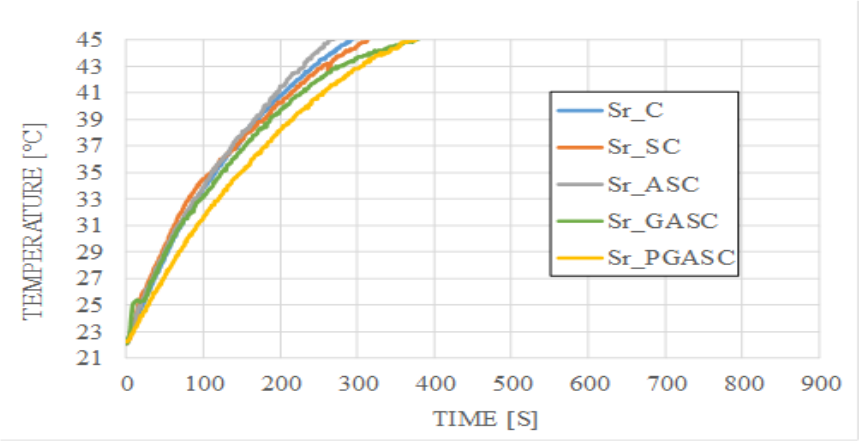

Figure 4.21 **:** Heating curves of Sr_C, Sr _SC, Sr _ASC, Sr _GASC, Sr _PGASC in water media as % 0.1 (v/m) equal ratio at 5 kW.

5. CONCLUSIONS

In this master thesis, $SrFe_{12}O_{19}$, $MnFe_2O_4$, $MgFe_2O_4$, Fe_3O_4 SPIONs with superior magnetic properties were produced and coated with silica, amination, gold and PEG to gain various functions. According to the characterization results, it can be said that the coatings have been achieved successfully. Magnetic heating performances at 5kW of all NP types that produced and each coating layer applied were examined separately.

According to the results of the magnetic heating experiments, among all samples, $SrFe_{12}O_{19}$ NPs showed the lowest and $MgFe_2O_4$ NPs showed the highest heating performance in the experiments that comparing different core types among all samples.

According to the heating results that comparing different coating stages, aminated NPs gave the high heating performance among other coating stages. This is a surprising and unintuitive result. The aminated NPs, in some way, showed an increasing effect on the heating performance in all multi-component NPs regardless of the core type. To the best of our knowledge, the results of this study have not been encountered before in the literature.

Comparing of different coating stages of NPs, PEG coated samples gave the slowest heating performance in the heating results. In addition, the heating performance of gold-coated samples, which is the previous coating step from PEG, was very close to that of PEG-coated NPs and gave the second lowest performance.

There are studies in the literature observed that gold coating increased the heating performance of the NPs relatively [28]. In our study, on the other hand; It can be mentioned that (a) the size of the NPs, the coating thicknesses are different and (b) the mixtures prepared for the heating experiments do not contain the same amount of NPs. In addition, in the study, NPs were characterized with EDX to prove that the existence of gold coating and gold content was found in all of them, but due to the possibility of insufficient washing after gold coating, it is not strange that gold peaks appeared in

the EDX even though gold coating failed. In order to obtain a more reliable result regarding the success of coatings stages and NPs sizes, it is recommended to conduct a characterization study with TEM.

As a result, the study has shown that differences of coating stages and differences of core types change the heating performance of superparamagnetic NPs. Although there are many studies on magnetic NPs in the literature, differently, the effects of different magnetic core types and different coating stages on heating performance were compared in standard laboratory conditions.

It is possible to say that this study, which is carried out with easily accessible and economical laboratory materials, is enlightening for future researches related to the subject.

REFERENCES

[1] **Cai, W., Gao, T., Hong, H., & Sun, J.** (2008). Applications of gold nanoparticles in cancer nanotechnology. Nanotechnology, Science and Applications, 1, 17–32.

[2] **Kievit, F. M., & Zhang, M.** (2011). Surface Engineering of Iron Oxide Nanoparticlesfor Targeted Cancer Therapy. Accounts of Chemical Research, 9, 9-99.

[3] **Laurent, S., Dutz, S., Häfeli, U. O., & Mahmoudi, M.** (2011). Magnetic fluid hyperthermia: Focus on superparamagnetic iron oxide nanoparticles. Advances in Colloid and Interface Science, 166, 8-23.

[4] **Roca1, A. G., Morales, M. P., Grady, K. O., & Serna, C. J.** (2006) Structural and magnetic properties of uniform magnetite nanoparticles prepared by high temperature decomposition of organic precursors. Nanotechnology, 17,2783–2788.

[5] **Sun, C., Lee, J. S. H., & Zhang, M.** (2008). Magnetic nanoparticles in MR imaging and drug delivery. Advanced Drug Delivery Reviews, 60, 1252–1265.

[6] **Ortega D. and Pankhurst Q. A.** (2013). Magnetic hyperthermia, in Nanoscience. Volume 1, Nanostructures through Chemistry, P. O'Brien, Editor. Royal Society of Chemistry. Cambridge, p. 60-88.

[7] **Ansari L. and Malaekeh-Nikouei B.** (2016). Magnetic silica nanocomposites for magnetic hyperthermia applications, International Journal of Hyperthermia. pages 354-363

[8] **Rashid AU., Southern P., Darr JA., Awan S., Manzoor S.** (2013). Strontium hexaferrite (SrFe12O19) based composites for hyperthermia applications. Journal of Magnetism and Magnetic Materials, Volume 344, October 2013, Pages 134-139, ISSN 0304-8853.

[9] **Sadhana K., Praveena K., Matteppanavar S., Angadi B.** (2012). Structural and magnetic properties of nanocrystalline BaFe12O19 synthesized by microwavehydrothermal method, Appl. Nanosci. 2 247e252.

[10] **Chen, D., Tang, Q., Li, X., Zhou, X., Zang, J., Xue, W., … Guo, C.** (2012). Biocompatibility of magnetic Fe3O4 nanoparticles and their cytotoxic effect on MCF-7 cells. International Journal of Nanomedicine, 7, 4973–4982.

[11] **Thai Y.T., Kim D.-H., Brazel C.S.** (2008). Heat Generation in Manganese Ferrite (MnFe2O4) Nanoparticles for Localized Hyperthermia Treatment of Cancer. JOSHUA.

[12]**Treatment Types**.(2021). Retrieved from https://www.cancer.org/treatment/treatments-and-side-effects.html

[13] **Chemotherapy.**(2021).Retrieved from https://www.cancerresearchuk.org/about-cancer/cancer-in-general/treatment/chemotherapy

[14] **Sudhakar, A.** (2009). History of Cancer, Ancient and Modern Treatment Methods. Journal of Cancer Science & Therapy, 1(2), 1–4.

[15] **Radiotherapy.**(2021).Retrieved from https://www.cancerresearchuk.org/about-cancer/cancer-in-general/treatment/radiotherapy

[16] **Soares P.I., Ferreira I.M., Igreja R.A., Novo C.M., Borges J.P**. (2012). Application of hyperthermia for cancer treatment: recent patents review. Recent Pat Anticancer Drug Discov.;7:64–73.

[17] **Surgery.** (2021).Retrieved from https://www.cancerresearchuk.org/about-cancer/cancer-in-general/treatment/surgery

[18] **Beik J., Abed Z., Ghoreishi F. S., Hosseini-Nami S., Mehrzadi S., Shakeri-Zadeh A., Kamrava S. K.** (2016). Nanotechnology in hyperthermia cancer therapy: From fundamental principles to advanced applications, Journal of Controlled Release, Volume 235, Pages 205-221, ISSN 0168-3659.

[19] **Yadollahpour A., Hosseini S. A.** (2016). Magnetic nanoparticle based hyperthermia: A review of the physiochemical properties and synthesis methods. International Journal of Pharmaceutical Research & Allied Sciences., Vol. 5 Issue 2, p242-246. 5p.

[20] **Habash, R. W. Y.** (2008). Bioeffects and therapeutic applications of electromagnetic energy. Boca Raton: CRC Press.

[21] **Chichel A., Skowronek J., Kubaszewska M., Kanikowski M.** (2007). Hyperthermia - Description of a method and a review of clinical applications. Reports of Practical Oncology and Radiotherapy, 12 (5) , pp. 267-275.

[22] **Haghniaz, R., Umrani, R. D., & Paknikar, K. M.** (2015). Temperature-dependent and time-dependent effects of hyperthermia mediated by dextrancoated La0.7Sr0.3MnO3: in vitro studies. International Journal of Nanomedicine, 10, 1609–1623.

[23] **Hilger I.** (2013). In vivo applications of magnetic nanoparticle hyperthermia, International Journal of Hyperthermia, 29:8, 828-834.

[24]**Chatterjee, D. K., Diagaradjane, P., & Krishnan, S. (2011). Nanoparticlemediated hyperthermia in cancer therapy.** Therapeutic Delivery, 2(8), 1001–1014.

[25] **Wust P, Hildebrandt B, Sreenivasa G, et al.** (2002). Hyperthermia in combined treatment of cancer. The Lancet Oncology; 3(8):487–497.

[26] **Vorst V. A., Rosen A., Kotsuka Y.** (2006). RF/Microwave Interaction with Biological Tissues, John Wiley and Sons, Inc., ISBN 978-0-47173277-8.

[27] **Behrouzkia, Z., Joveini, Z., Keshavarzi, B., Eyvazzadeh, N., & Aghdam, R. Z.** (2016). Hyperthermia: How Can It Be Used? Oman Medical Journal, 31(2), 89–97.

[28] **Aydın E.** (2017). Multi-Component Superparamagnetic Nanoparticles For Cancer Therapy Via Hyperthermia, M.Sc. Thesis, Department of Electronics and Communication Engineering Biomedical Engineering Programme, Istanbul Technical University.

[29] **Obaidat, I., Issa, B., & Haik, Y.** (2015). Magnetic Properties of Magnetic Nanoparticles for Efficient Hyperthermia. Nanomaterials, 5(1), 63– 89.

[30] **Levy A.** (2009). Early Detection Of Tumors Using Infrared Imaging And Antibodies Conjugated Magnetic Nanoparticles. M.Sc. Thesis, Tel Aviv University The Iby and Aladar Fleischman Faculty of Engineering The Zandman-Slaner School of Graduate Studies.

[31] **Karkan S. F., Mohammadhosseini M., Panahi Y., Milani M., Zarghami N., Akbarzadeh A., Abasi E., Hosseini A., Davaran S.** (2016). Magnetic nanoparticles in cancer diagnosis and treatment: a review, Artificial Cells, Nanomedicine, and Biotechnology. Pages 1-5

[32] **Kolhatkar, A. G., Jamison, A. C., Litvinov, D., Willson, R. C., & Lee, T. R.** (2013). Tuning the Magnetic Properties of Nanoparticles. International Journal of Molecular Sciences, 14, 15977-16009.

[33] **Köktitz, R., Weitschies, W., Trahms, L., & Semmler, W.** (1999). Investigation of Brownian and NeHel relaxation in magnetic fluids. Journal of Magnetism and Magnetic Materials, 201, 102-104.

[34] **Suto, M., Hirota, Y., Hiroaki, M., Fujit, A., Kasuya, R., Tohji, K., & Jeyadevan, B.** (2009). Heat dissipation mechanism of magnetite nanoparticles in magnetic fluid hyperthermia. Journal of Magnetism and Magnetic Materials, 321, 1493–1496.

[35] **Wendt, M., & Ergun, C.,** (2014). Magnetic heating of smart nanoparticles embedded in agar – influence of magnetic core and surfacedemodifications on the heating performance. (Master Thesis). Department of Mechanical Engineering, Istanbul Technical University, Istanbul.

[36] **Mohapatra, M., & Anand, S.** (2010). Synthesis and applications of nanostructured iron oxides/hydroxides– a review. International Journal of Engineering, Science and Technology, 2(8), 127-146.

[37] **Drmota, A. Drofenik,M. Koselj, J. and Žnidaršič, A. Edited by Dr. Najjar, R.** (2012). Microemulsion Method for Synthesis of Magnetic Oxide Nanoparticles. Microemulsions - An Introduction to Properties and Applications, Chapter 10.

[38] **Santra, S., Tapec, R., Theodoropoulou, N., Dobson, J., Hebard, A.i & Tan, W.** (2001). Synthesis and Characterization of Silica-Coated Iron Oxide Nanoparticles in Microemulsion: The Effect of Nonionic Surfactants. American Chemical Society 17, 2900-2906.

[39] **Ding, H. L., Zhang, Y. X., Wang, S., Xu, J. M., Xu, S. C., & Li, G. H.** (2012). Fe3O4@SiO2 Core/Shell Nanoparticles: The silica soating regulations with a single core for different core sizes and shell thicknesses. American Chemical Society, 24, 4572−4580.

[40] **Faraji, M., Yamini, Y. & Rezaee, M.** (2010). Magnetic nanoparticles: Synthesis, stabilization, functionalization, characterization, and applications. Department of Chemistry, Tarbiat Modares University. J. Iran. Chem. Soc., Vol. 7, No. 1, March 2010, pp. 1-37

[41] **Lu, A., Salabas, E. L., & Schüth, F**. (2007). Magnetic Nanoparticles: Synthesis, Protection, Functionalization, and Application. Magnetic Nanoparticles, 46, 1222 – 1244.

[42] **Marinin A.** (2012). Synthesis and characterization of superparamagnetic iron oxide nanoparticles coated with silica, M.Sc. Thesis, Division of Functional Materials School of Information and Communication Technology Royal Institute of Technology, Stockholm.

[43] **Laurent S., Forge D., Port M., Roch A., Robic C., Elst L. V., and Muller R. N.** (2008). Magnetic Iron Oxide Nanoparticles: Synthesis, Stabilization, Vectorization, Physicochemical Characterizations, and Biological Applications, Chemical Reviews 108 (6), 2064-2110

[44] **Kim, K. H., Kim. M. J., Choa, Y. H. Kim, D. H., & Yu, J. H**, (2008). Synthesis and Magnetic Properties of Surface Coated Magnetite Superparamagentic Nanoparticles. IEEE Transacations on Magnetics, 44(11), 2940-2943.

[45] **Kim, D. K., Zhang, Y., Voit, W., Rao, K. V., & Muhammed, M.** (2001). Synthesis and characterization of surfactant-coated superparamagnetic monodispersed iron oxide nanoparticles. Journal of Magnetism and Magnetic Materials, 225, 30-36.

[46] **Sun, S. & Zeng, H.** (2002). Size-controlled cynthesis of magnetite nanoparticles. Journal of the American Chemical Society, 124, 8204-8205.

[47] **Sun, J., Zhou, S. Hou,P., Yang, Y., Weng, J., Li, X., & Li, M.** (2006). Synthesis and characterization of biocompatible Fe3O4 nanoparticles. Journal of Biomedical Materials Research Part A.

[48] **Hariani, P. L., Faizal, M., Marsi, R., & Setiabudidaya, D.** (2013). Synthesis and properties of Fe3O4 nanoparticles by co-precipitation method to removal procion dye. International Journal of Environmental Science and Development, 4(3), 336-340.

[49] **Kang, Y. S., Risbud, S., Rabolt, J. F., & Stroeve, P.,** (1996). Synthesis and characterization of nanometer-size Fe3O4 and Fe2O3 particles. Chemistry of Materials, 8(9), 2209-2211.

[50] **Petcharoena, K. & Sirivat, A.** (2012). Synthesis and characterization of magnetite nanoparticles via the chemical co-precipitation method. Journal of Materials Science and Engineering, 177, 421– 427.

[51] **Gnanaprakash, G., Mahadevan, S., Jayakumar, T., Kalyanasundaram, P., Philip, J., & Raj, B.** (2007). Effect of initial pH and temperature of iron salt solutions on formation of magnetite nanoparticles. Materials Chemistry and Physics, 103, 168–175.

[52] **Figuerola, A., Corato, R. D., Manna, L., & Pellegrino, T.** (2010). From iron oxide nanoparticles towards advanced iron-based inorganic materials

designed for biomedical applications. Pharmacological Research, 62, 126–143.

[53] **Hong, R. Y., Li, J. H., Zhang, S. Z., Li, H. Z., Zheng, Y., Ding, J., & We, D. G.** (2009). Preparation and characterization of silica-coated Fe3O4 nanoparticles used as precursor of ferrofluids. Applied Surface Science, 255, 3485–3492

[54] **Mascolo, M. C., Pei, Y., and Ring, T. A.,** (2013). Room temperature coprecipitation synthesis of magnetite nanoparticles in a large pH window with different bases. Journal of Materials, 6, 5549-5567.

[55] **Weia, Y., Hanb, B., Hua, X., Linc, Y., Wangd, X., & Denga, X.** (2011). Synthesis of Fe3O4 nanoparticles and their magnetic properties. Chinese Materials Conference,. 27, 632 – 637.

[56] **Shen, Y. F., Tang, J., Nie, Z. H., Wang, Y. D., Ren, Y., & Zuo, L.,** (2009). Preparation and application of magnetic Fe3O4 nanoparticles for wastewater purification. Journal of Separation and Purification Technology, 68, 12–319.

[57] **Chen, C. L., Zhang, H., Ye, Q., Hsieh, W. Y., Hitchens, T. K., Shen, H. H., Liu, L., Wu, Y., J. Foley, L. M., Wang, S. J., & Ho, C.** (2011). A new nano-sized iron oxide particle with high sensitivity for cellular magnetic resonance imaging. Journal of Molecular Imaging and Society for Molecular Imaging, 13, 825-839.

[58] **Omer, M., Haider, S., & Park, S. Y.** (2011). A novel route for the preparation of thermally sensitive core-shell magnetic nanoparticles. Journal of Polymer, 52. 9197.

[59] **Guerrero-Martinez, B. A., Perez-Juste, J., & Liz-Marzan, L. M.** (2010). Recent progress on silica coating of nanoparticles and related nanomaterials. Journal of Advanced Materials, 22, 1182–1195.

[60] **Ammar, M., Mazaleyrat, F., Bonnet, J. P., Audebert, P., Brosseau, A., Wang, G., & Champion, Y.** Synthesis and characterization of coreshell structure silicacoated Fe29.5Ni70.5 nanoparticles.

[61] **Johnson, N. J. J., Sangeetha, N. M., Boyer, J. C., & Veggel, F. C. J. M.,** (2010). Facile ligand-exchange with polyvinylpyrrolidone and subsequent silica coating of hydrophobic upconverting b- NaYF4:Yb3+/Er3+ nanoparticles. Journal of the Royal Society of Chemistry, 2, 771–777.

[62] **Jana, N. R., Earhart, C., & Ying, J. Y.** (2007). Synthesis of water-soluble and functionalized nanoparticles by silica coating. Journal of American Chemical Society, 19(21), 5074-5082.

[63] **Ji, X., Shao, R., Elliott, A. M., Stafford, R. J., Esparza-Coss, E., Bankson, J. A., Liang, G., Luo, Z. P., Park, K., Markert, J. T., & Li, C.** (2007). Bifunctional gold nanoshells with a superparamagnetic iron oxide-silica core suitable for both MR imaging and photothermal therapy. The Journal of Physical Chemistry, 111, 62456251.

[64] **Deng, Y. H., Wang, C. C., Hu, J. H., Yang, W. L., & Fu, S. K.** (2005). Investigation of formation of silica-coated magnetite nanoparticles via sol–gel approach. Journal of Colloids and Surfaces A, 262, 87–93.

[65] **Dick, K., Dhanasekaran, T., Zhang, Z., & Meisel, D.,** (2002). Size-dependent melting of silica-encapsulated gold nanoparticles. Journal of American Chemistry Society, 124(10), 2312-2317.

[66] **Yi, D. K., Selvan, S. T., Lee, S. S., Papaefthymiou, G. C., Kundaliya, D. & Ying, J. Y.** (2005). Silica-coated nanocomposites of magnetic nanoparticles and quantum dots. Journal of American Chemistry Society, 127, 4990-4991.

[67] **Kobayashi, Y., Horie, M., Konno, M., Rodriguez-Gonzalez, B., & LizMarzan, L. M.** (2003). Preparation and properties of silica-coated cobalt nanoparticles. The Journal of Physical Chemistry B., 107, 7420-7425.

[68] **Kobayashi, Y., Katakami, H., Mine, E., Nagao, D., Konno, M., & LizMarz n, L. M.** (2005). Silica coating of silver nanoparticles using a modified Stöber method. Journal of Colloid and Interface Science,283, 392–396.

[69] **Lopez, C. F., Mateo, C. M., Alvarez-Puebla, R. A., Perez-Juste, J., Pastoriza-Santos, I., & Liz-Marzan, L. M.** (2009). Highly controlled silica coating of PEG-capped metal nanoparticles and preparation of SERS-encoded particles. Journal of Langmuir, 25(24), 13894–13899.

[70] **Lu, Y., Yin, Y., Mayers, B. T., & Xia, Y.** (2001). Modifying the surface properties of superparamagnetic iron oxide nanoparticles through a sol-gel approach. Journal of Nano Letters, 2(3), 183-186.

[71] **Ghasemia, E., Ghaharia, M., Mehranpoor, N., & Mirhabibi, A.** (2012). Silica coated magnetite nanoparticles: effects of TEOS concentration. Proceedings of the 4th International Conference on Nanostructures (ICNS4).

[72] **Ibrahim, I. A. M., Zikry, A.A.F., & Sharaf, M. A.** (2010). Preparation of spherical silica nanoparticles: Stober silica. Journal of American Science, 6(11), 985-989.

[73]**Lin, J.** (2001). Gold-coated iron (Fe@Au) nanoparticles: synthesis, characterization, and magnetic field-induced aelf-assembly. Journal of Solid State Chemistry, 159, 26-31 .

[74] **Otoufi, M. K., Shahtahmasebebi, N., Kompany, A., & Goharshadi, E.** (2014). A systematic growth of gold nanoseeds on silica for silica@gold core-shell nanoparticles and investigation of optical properties. International Journal of Nano Dimension, 5(6),525-531.

[75] **Khosroshahi, M. E., & Nourbakhsh, M. S.** (2010). Preparation and characterization of self assembled gold nanoparticles on amino functionalized SiO2 dielectric core. International Journal of Chemical, Molecular, Nuclear, Materials and Metallurgical Engineering, 4(4), 264-267.

[76] **Kouassi, G. K., & Irudayaraj, J.** (2006). Magnetic and gold-coated magnetic nanoparticles as a DNA sensor. Journal of American Chemical Society, 10, 32343241.

[77] **Yamauraa, M., Camiloa, R. L., Sampaiob, L. C., Macedoc, M. A., Nakamurad, M., & Toma, H. E.** (2004) Preparation and

characterization of (3aminopropyl) triethoxysilane-coated magnetite nanoparticles. Journal of Magnetism and Magnetic Materials, 279, 210–217.

[78] **Chen, M., Yamamuro, S., Farrell, D., and Majetich, S. A.** (2003). Goldcoated iron nanoparticles for biomedical applications. Journal of Applied Physics, 93, 7551-7553.

[79] **Pal, S., Morales, M., Mukherjee, P., & Srikanth, H.** (2009) Synthesis and magnetic properties of gold coated iron oxide nanoparticles. Journal of Applied Physics, 105, 07B504.

[80] **Madhuri, M., Kundu, S., Ghosh, S. K., Panigrahi, S., Sau, T. K., Yusuf, S. M., & Pal, T.** (2005). Magnetite nanoparticles with tunable gold or silver shell. Journal of Colloid and Interface Science, 286, 187–194.

[81] **Salehizadeh, H., Hekmatian, E., Sadeghi, M., & Kennedy, K.,** (2012). Synthesis and characterization of core-shell Fe3O4-gold-chitosan nanostructure. Journal of Nanobiotechnology, 10(3).

[82] **Lo, C. K., Xiao, D., & Choi, M. M. F.** (2007). Homocysteine-protected goldcoated magnetic nanoparticles: synthesis and characterisation. Journal of Materials Chemistry, 17, 2418–2427.

[83] **Rahman, M. T., Krishnamurthy, P. G., Parthiban, P., Jain, A., Park, C. P., Kim, D. P., & Khan, S. A.** (2013). Dynamically tunable nanoparticle engineering enabled by short contact-time microfluidic synthesis with a reactive gas. Journal of Electronic Supplementary Material.

[84] **Cho, S. J., Idrobo, J. C., Olamit, J., Liu, K., Browning, N. D., & Kauzlarich, S. M.** Growth mechanisms and oxidation-resistance of gold-coated iron nanoparticles.

[85] **Park, S. E., Park, M. Y., Han, P. K., & Lee, S. W.** (2006) The effect of pHadjusted gold colloids on the formation of gold clusters over APTMS-coated silica cores. Journal of Korean Chemical Society, 27(9), 1341-1345.

[86] **Hodenius, M., Hieronymus, T., Zenke, M., Becker, C., Elling, L., Bornemann, J., Wong, J. E., Richtering, W., Himmelreich, U., & Cuyper, M.,** (2012). Magnetically triggered clustering of biotinylated iron oxide nanoparticles in the presence of streptavidinylated enzymes. Journal of Nanotechnology, 23, 9.

[87] **Qu, J. B., Shao, H. H., Jing, G. L., & Huang, F.,** (2013). PEG-chitosancoated iron oxide nanoparticles with high saturated magnetization as carriers of 10 hydroxycamptothecin: Preparation, characterization and cytotoxicity studies. Journal of Colloids and Surfaces B, 102, 37– 44

[88] **Fenga, B., Hong, R.Y., Wanga, L.S., Guoc, L., Lib, H.Z., Dingd, J., Zhenge, Y., & Wei, D.G.** (2008). Synthesis of Fe3O4/APTES/PEG diacid functionalized magnetic nanoparticles for MR imaging. Journal of Colloids and Surfaces A, 328, 52–59

[89] **Zhang, Y., Kohler, N., & Zhang, M.** (2002). Surface modification of superparamagnetic magnetite nanoparticles and their intracellular uptake. Journal of Biomaterials, 23, 1553–1561.

[90] **Chen, T. J., Cheng, T. H., Hung, Y. C., Lin, K.T., Liu, G. C., & Wang, Y. M.,** (2007). Targeted folic acid-PEG nanoparticles for noninvasive imaging of folate receptor by MRI. Wiley InterScience, 165-175.

[91] **Park, J. Y., Daksha, P., Lee, G. H., Woo, S., & Chang, Y.** (2008). Highly water-dispersible PEG surface modified ultra small superparamagnetic iron oxide nanoparticles useful for target-specific biomedical applications. Journal of Nanotechnology, 19.

[92] **Herve, K., Douziech-Eyrolles, L., Munnier, E., Cohen-Jonathan, S., Souce, M., Marchais, H., Limelette, P., Warmont, F., Saboungi, M. L., Dubois, P., & Chourpa, I.** (2008). The development of stable aqueous suspensions of PEGylated SPIONs for biomedical applications. Journal of Nanotechnology, 19.

[93] **Sun, C., Veiseh, O., Gunn, J., Fang, C., Hansen, S., Lee, D., Sze, R., Richard G., Ellenbogen, J. O., & Zhang, M**. (2008). In vivo MRI detection of gliomas by chlorotoxin-conjugated superparamagnetic nanoprobes. Small Journal, 3, 372 – 379.

[94] **Xie, B. J., Xu, C., Kohler, N., Hou, Y., & Sun, S.** (2007). Controlled PEGylation of Monodisperse Fe3O4 Nanoparticles for Reduced Non-Specific Uptake by Macrophage Cells. Journal of Advanced Materials, 19, 3163–3166.

[95] **Umut E.** (2013). Surface Modification of Nanoparticles Used in Biomedical Applications, Modern Surface Engineering Treatments, Dr. M. Aliofkhazraei (Ed.), InTech. DOI: 10.5772/55746.

[96] **Saniei N.** (2009). Hyperthermia and Cancer Treatment, Heat Transfer Engineering, 30:12, 915-917.

[97] **Barry, S. E.** (2008). Challenges in the development of magnetic particles for therapeutic applications. Int. J. Hyperthermia 24, 451–466.

[98] **Nejatpour M.** (2016). Synthesize And Characterization Of Multi-Component Magnetic Nano Particles, M.Sc. Thesis, Department of Mechanical Engineering Materials and Manufacture Program, Istanbul Technical University.

[99] **Mohammad-Beigi H., Yaghmaei S., Roostaazad R., Arpanaei A.** (2013) Comparison of different strategies for the assembly of gold colloids onto Fe3O4@SiO2 nanocomposite particles, Physica E: Lowdimensional Systems and Nanostructures, Volume 49, Pages 30-38, ISSN 1386-9477.

[100] **Pham T., Jackson J. B., Halas N. J. and Lee T. R.** (2002) Preparation and Characterization of Gold Nanoshells Coated with Self-Assembled Monolayers. Langmuir 18 (12), 4915-4920.

[101] **Yucesoy A.** (2014). Synthesis of gold nanoparticles for cancer therapeutic applications. B.S. Thesis. Biomedical Engineering in the Department of Biomedical Engineering, Georgia Institute of Technology. USA.

[102] **Hong, R. Y., Zhang, S. Z., Di, G. Q., Li, H. Z., Zheng, H. Z. Ding, J., & Wei, D. G.** (2008). Preparation, charaterization and application of

Fe3O4/ZnO core/shell magnetic nanoparticles, Materials Research Bulletin, 42, 2457-2468.

[103] **Chen, L., Xu, Z., Dai, H., & Zhang, S.,** (2010). Facile synthesis and magnetic properties of monodisperse Fe3O4/silica nanocomposite microshperes with embedded structures via a direct solution-based route, Journal of Alloys and Composites, 497, 221-227. 46

[104] **Hu, H., Wang, Z., & Pan, L.** (2010). Synthesis of monodisperse Fe3O4@silica core-shell microspheres and their application for removal of heavy ions from water, Journal of Alloys and Compounds, 492, 656-661.

[105] **Chen, F. H., Gao, Q., & Ni, J. Z.** (2008) The grafting and release behavior of doxorubincin from Fe3O4@SiO2 core-shell structure nanoparticles via an acid cleaving amide bond: The potential for magnetic targeting drug delivery, Nanotechnology, 19, 1-9.

[106] **Meng, X., Zhu, Y., Xu, S., & Liu, T.** (2016). Facile synthesis of shell-core polyaniline/SrFe12O19, Journal of Royal Society of Chemistry, 4946-4949

[107] **Meng, Y. Y., He, M. H., Zeng, Q., Jiao, D. L., Shukla, S., Ramanujan, R. V., & Liu, Z. W.** (2014) Synthesis of barium ferrite ultrafine powders by a sol–gel combustion method using glycine gels, Journal of Alloys and Compounds, 220–225.

[108] **Khot, V. M., Salunkhe, A. B., Thorat, N. D., Ningthoujam, R. S., & Pawar, S. H.** (2013) Induction heating studies of dextran coated MgFe2O4 nanoparticles for magnetic hyperthermia, Journal of Dalton Transactions, 1249–1258.

[109] **Bangale, S. V., Patil, D. R., & Bamane, S. R.** (2011) Preparation and electrical properties of nanocrystalline MgFe2O4 oxide by combustion route. Archives of Applied Science Research, 3, 506-513.

[110] **Xu, Y., Sherwood, J., Qin, Y., Hollerc, R. A., & Bao, Y.** (2015) A general approach to the synthesis and detailed characterization of magnetic ferrite nanocubes, Journal of Royal Society of Chemistry, 7, 12641–12649.

[111] **Hosseini, S. H. & Asadnia, A.** (2012) Synthesis, Characterization, and Microwave-Absorbing Properties of Polypyrrole/MnFe2O4 Nanocomposite , Journal of Nanomaterials, Article ID 198973.

[112] **Zhang, L., He, R., & Gu, H. C.,** (2006) Oleic acid coating on the monodisperse magnetic nanoparticles. Applied Surface Science, no. article in press, 2006. 47

[113] **Mahdavi, M., Ahmad, M. B., Haron, M. J., Namvar, F., Nadi, B. Rahman, M. Z., & Amin, J.** (2013) Synthesis, surface modification and characterization of biocompatimble magnetic iron oxide nanoparticles for biomedical applications, Molecules, 7533-7548.

[114] **Lambert, J. B.** (1987). Introduction to organic spectroscopy, New York: Macmillan.

[115] **Manson, J., Kumar, D., Meenan, B. J., & Dixon, D.** (2011). Polyethylene glycol functionalized gold nanoparticles: the influence of capping density on stability in various media. Gold bulletin, 44(2), 99-105.

[116] **Ji, X., Shao, R., Elliott, A. M., Stafford, R. J., Esparza-Coss, E., Bankson, J. A., … Li, C.** (2007). Bifunctional Gold Nanoshells with a Superparamagnetic Iron Oxide-Silica Core Suitable for Both MR Imaging and Photothermal Therapy. The Journal of Physical Chemistry. C, Nanomaterials and Interfaces, 111(17), 6245–6251.

[117] **Hoskins, C., Min, Y., Gueorguieva, M., McDougall, C., Volovick, A., Prentice, P., … Wang, L.** (2012). Hybrid gold-iron oxide nanoparticles as a multifunctional platform for biomedical application. Journal of Nanobiotechnology, 10, 27.

APPENDICES

APPENDIX A : SEM images of SPIONs.
APPENDIX B : EDX results of SPIONs.

APPENDIX A

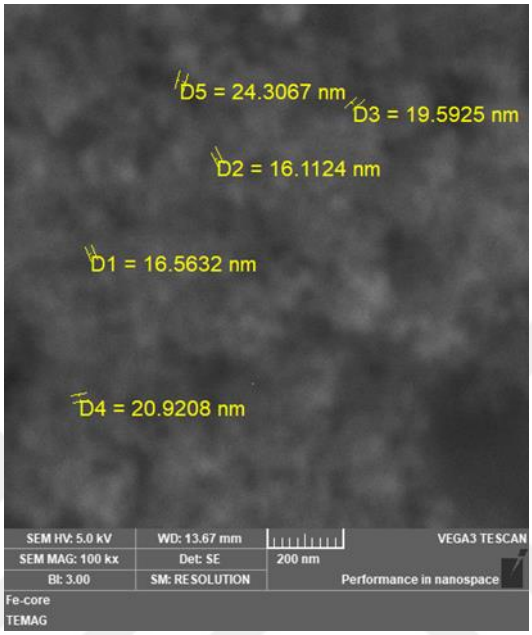

Figure A.1 : SEM images of Fe_C

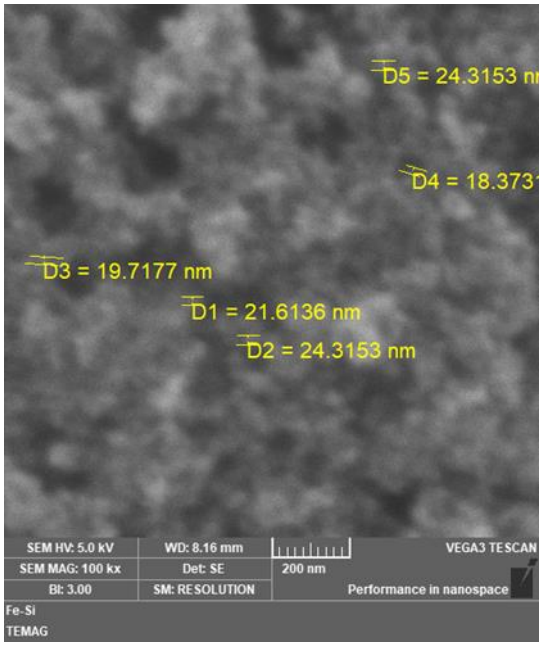

Figure A.2 : SEM images of Fe_SC

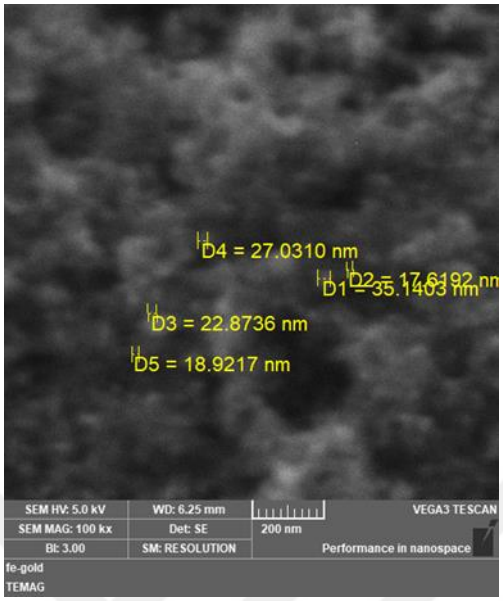

Figure A.3 : SEM images of Fe_GASC

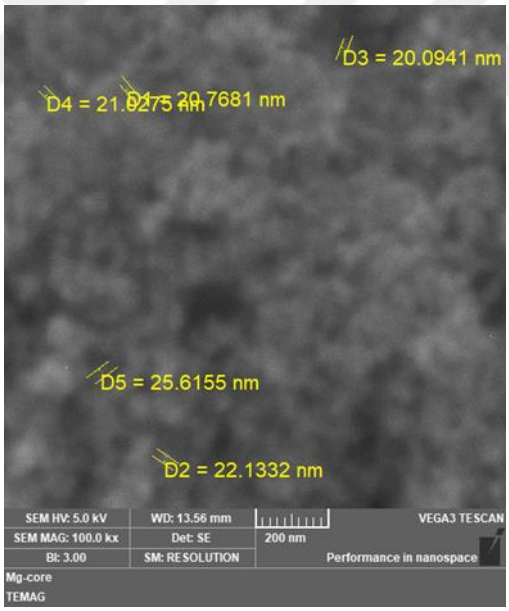

Figure A.4 : SEM images of Mg_C

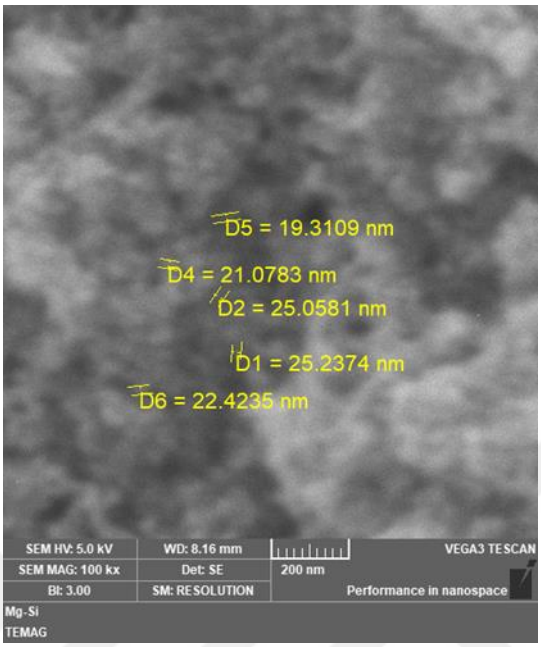

Figure A.5 : SEM images of Mg_SC

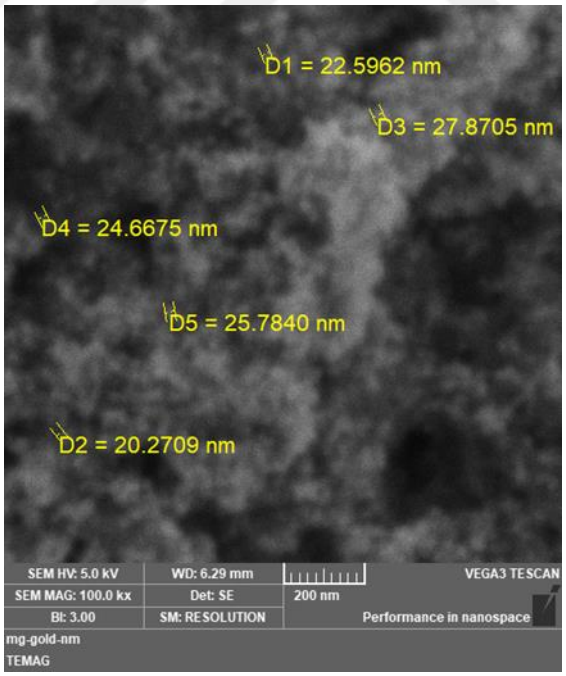

Figure A.6 : SEM images of Mg_GASC

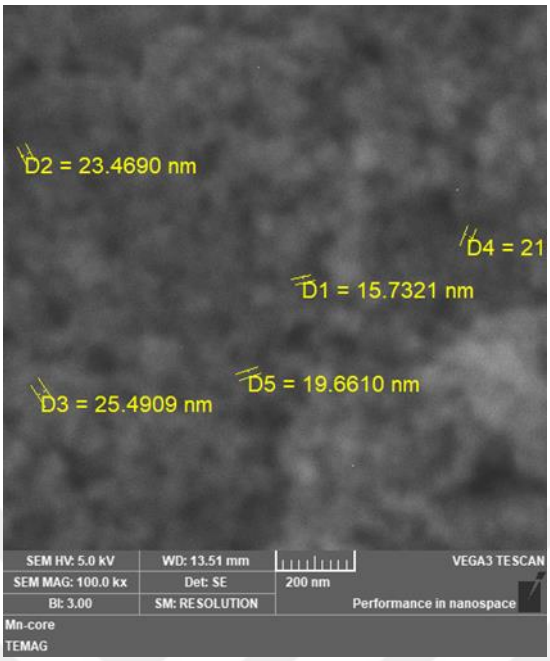

Figure A.7 : SEM images of Mn_C

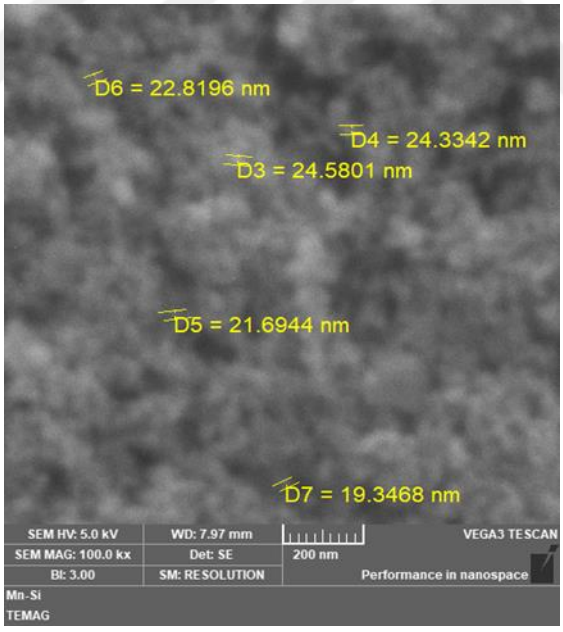

Figure A.8 : SEM images of Mn_SC

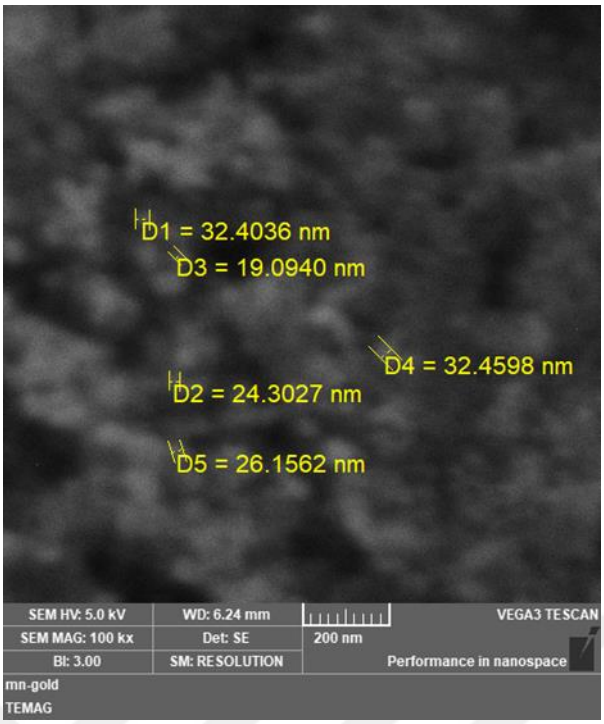

Figure A.9 **:** SEM images of Mn_GASC

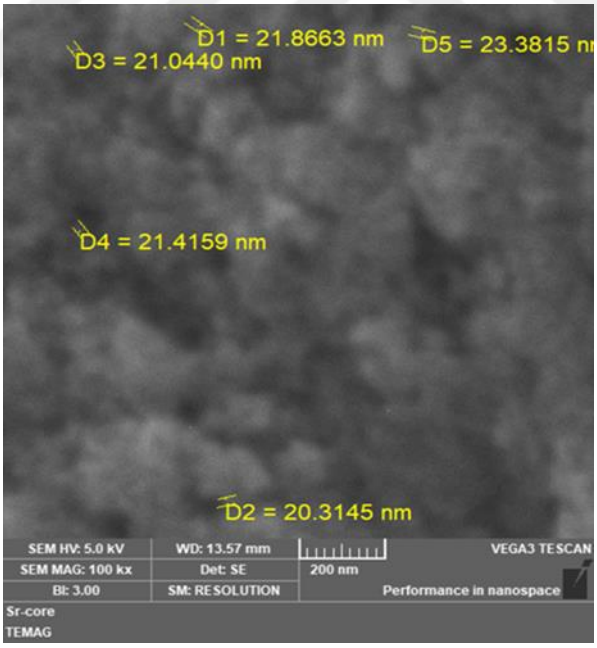

Figure A.10 **:** SEM images of Sr_C

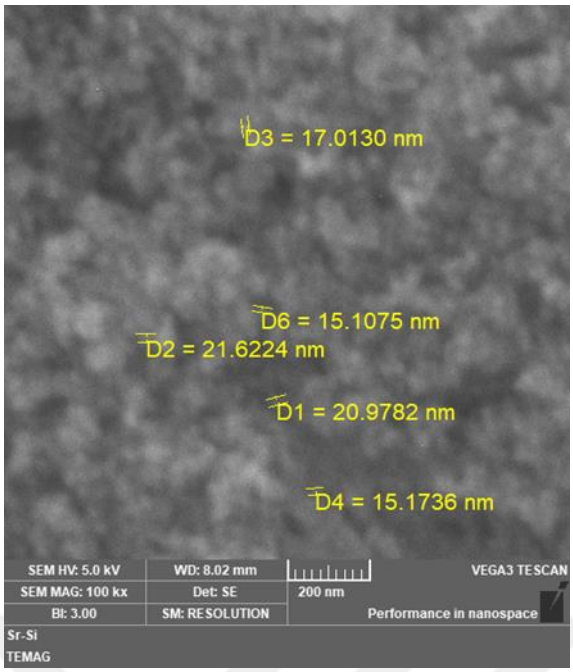

Figure A.11 : SEM images of Sr_SC

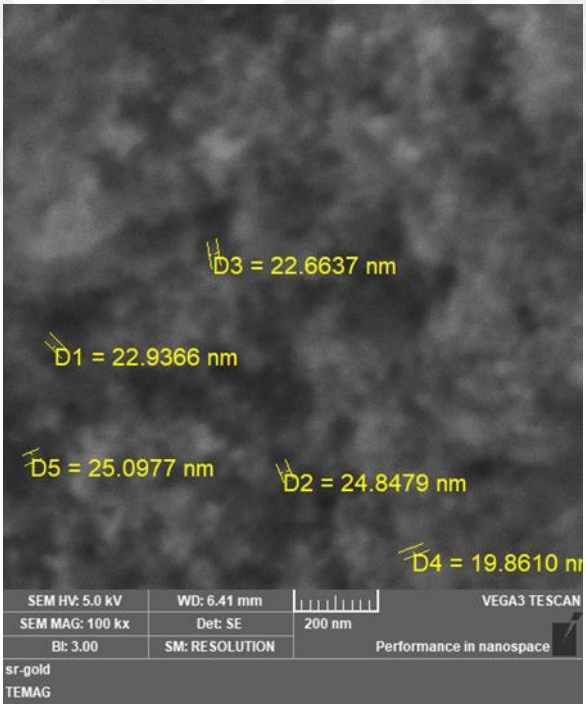

Figure A.12 : SEM images of Sr_GASC

APPENDIX B

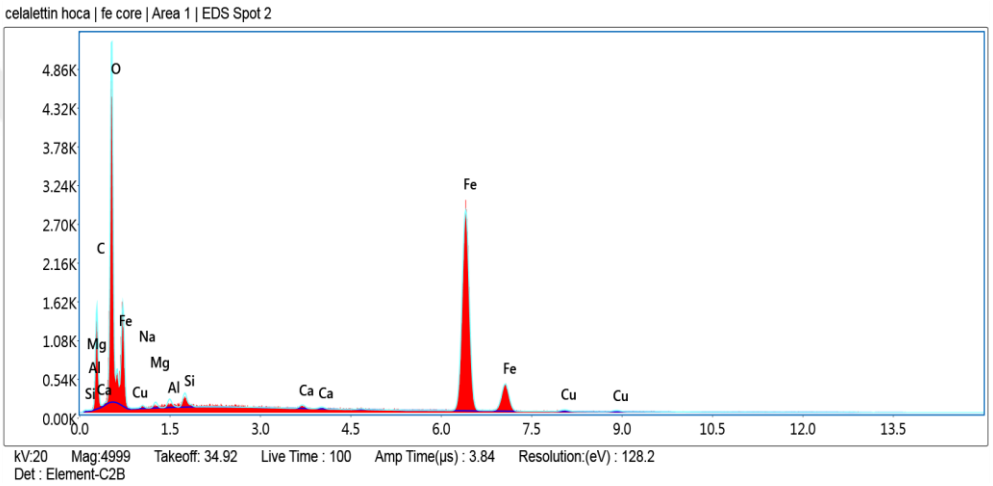

Element	Weight %	Atomic %	Error %
C K	20.30	33.60	9.40
O K	41.40	51.50	8.20
Fe L	34.20	12.20	8.90
Na K	0.50	0.40	50.80
Mg K	0.60	0.50	22.90
Al K	0.80	0.60	15.70
Si K	1.00	0.70	10.30
Ca K	0.40	0.20	29.80
Cu K	0.80	0.20	26.50

Figure B.1 : EDX of Fe_C

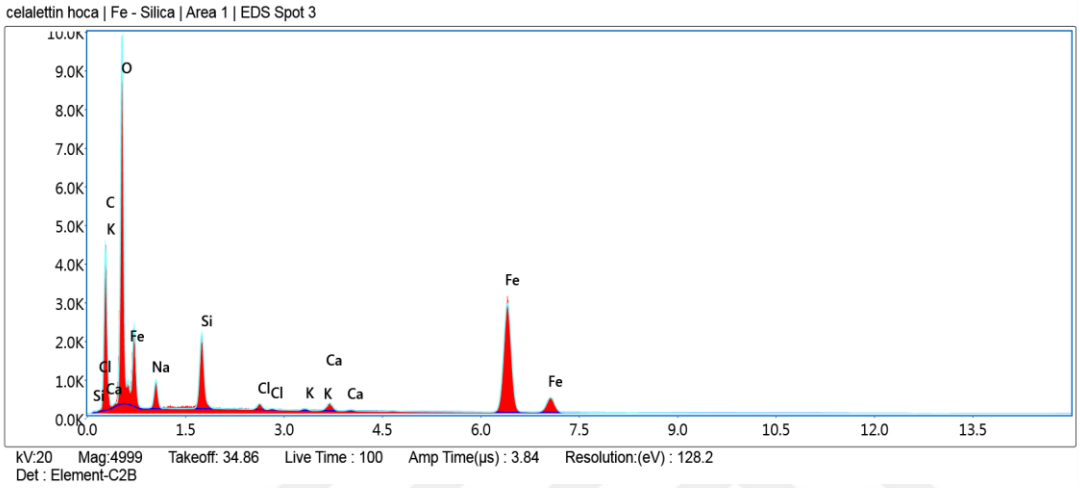

Element	Weight %	Atomic %	Error %
C K	27.50	42.10	8.60
O K	37.70	43.30	8.70
Na K	3.70	3.00	11.30
Si K	3.80	2.50	5.50
Cl K	0.40	0.20	15.70
K K	0.10	0.10	29.80
Ca K	0.70	0.30	10.90
Fe K	26.00	8.60	2.20

Figure B.2 : EDX of Fe_SC

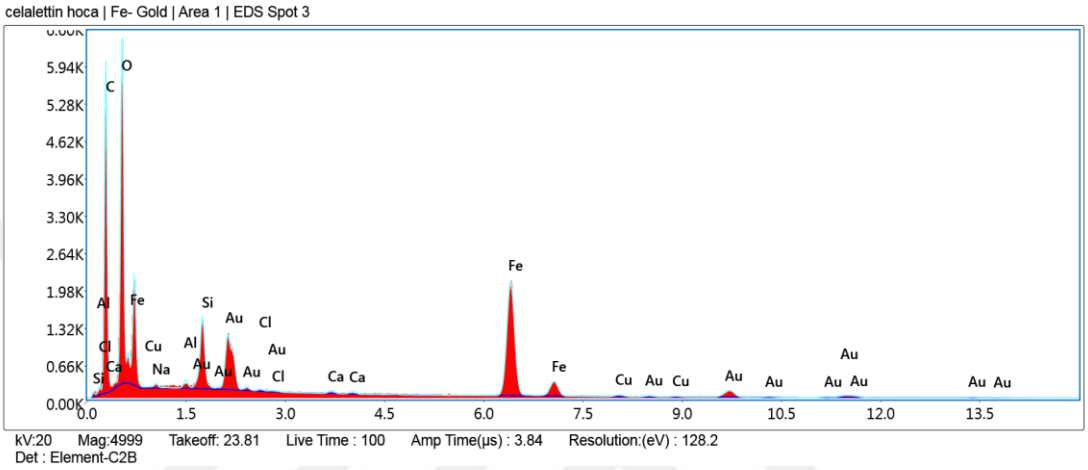

Element	Weight %	Atomic %	Error %
C K	33.00	51.90	8.20
O K	31.80	37.60	9.30
Na K	0.30	0.30	40.00
Al K	0.40	0.20	15.30
Si K	2.60	1.80	5.90
Cl K	0.10	0.00	66.90
Ca K	0.20	0.10	23.10
Fe K	20.00	6.80	2.40
Cu K	0.50	0.10	34.70
Au L	11.10	1.10	16.90

Figure B.3 : EDX of Fe_GASC

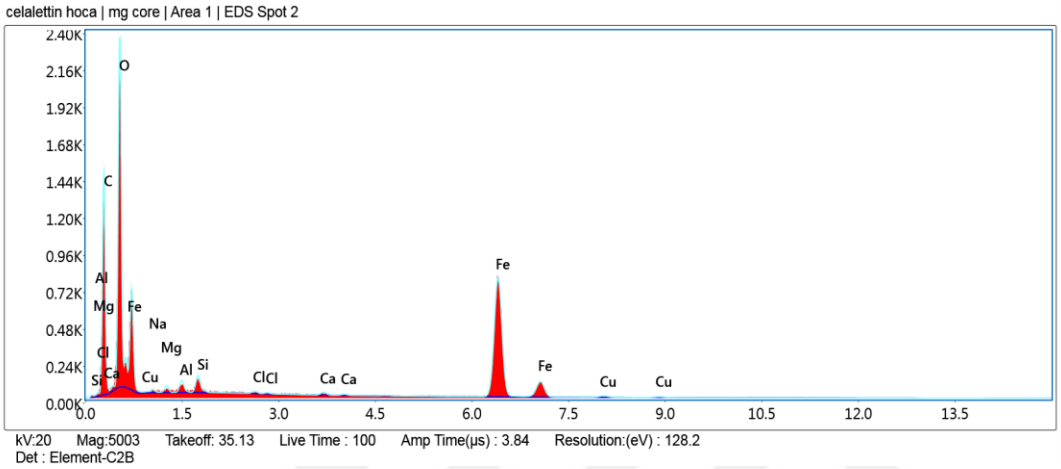

Element	Weight %	Atomic %	Error %
C K	30.40	46.20	8.20
O K	36.90	42.10	8.70
Na K	0.40	0.30	37.80
Mg K	0.50	0.40	16.30
Al K	0.80	0.50	11.00
Si K	0.90	0.60	8.20
Cl K	0.20	0.10	31.80
Ca K	0.30	0.10	21.00
Fe K	29.00	9.50	2.30
Cu K	0.60	0.20	23.50

Figure B.4 : EDX of Mg_C

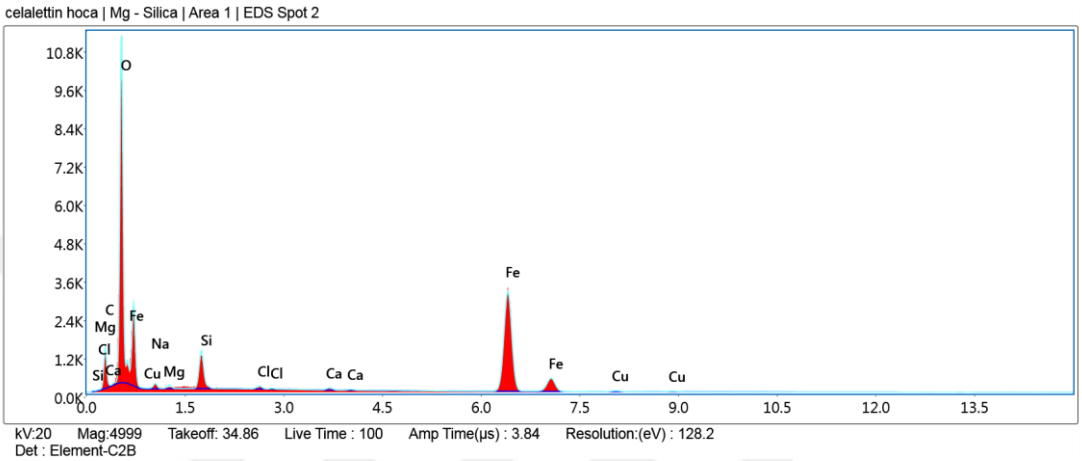

Element	Weight %	Atomic %	Error %
C K	11.60	21.50	9.80
O K	41.10	57.10	7.30
Na K	1.30	1.20	21.40
Mg K	0.50	0.50	18.90
Si K	3.60	2.90	6.60
Cl K	0.40	0.20	21.30
Ca K	0.40	0.20	18.80
Fe K	40.50	16.10	2.10
Cu K	0.70	0.30	22.00

Figure B.5 : EDX of Mg_SC

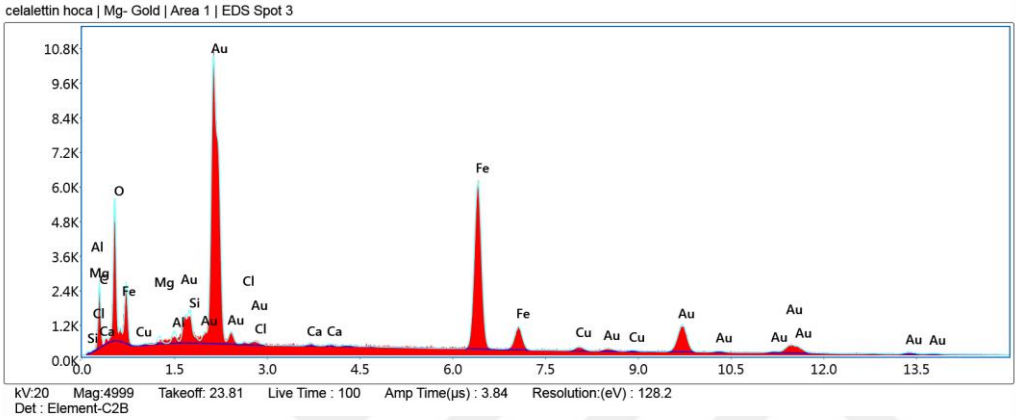

Element	Weight %	Atomic %	Error %
C K	8.60	29.90	10.70
O K	12.70	33.10	9.80
Mg K	0.50	0.90	20.10
Al K	0.60	1.00	14.10
Si K	1.40	2.00	8.00
Cl K	0.10	0.10	94.90
Ca K	0.30	0.30	43.00
Fe K	30.40	22.70	2.90
Cu K	1.10	0.70	27.30
Au L	44.30	9.40	9.60

Figure B.6 : EDX of Mg_GASC

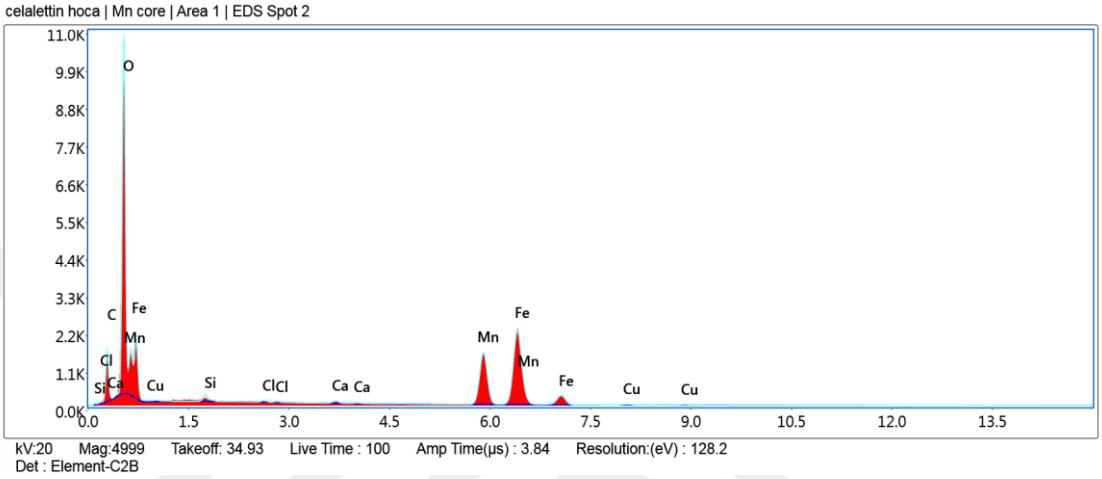

Element	Weight %	Atomic %	Error %
C K	12.40	23.60	9.40
O K	39.80	56.60	7.20
Fe L	28.50	11.60	9.70
Si K	0.60	0.50	10.50
Cl K	0.20	0.10	31.50
Ca K	0.40	0.20	23.30
Mn K	17.50	7.20	2.70
Cu K	0.50	0.20	33.20

Figure B.7 : EDX of Mn_C

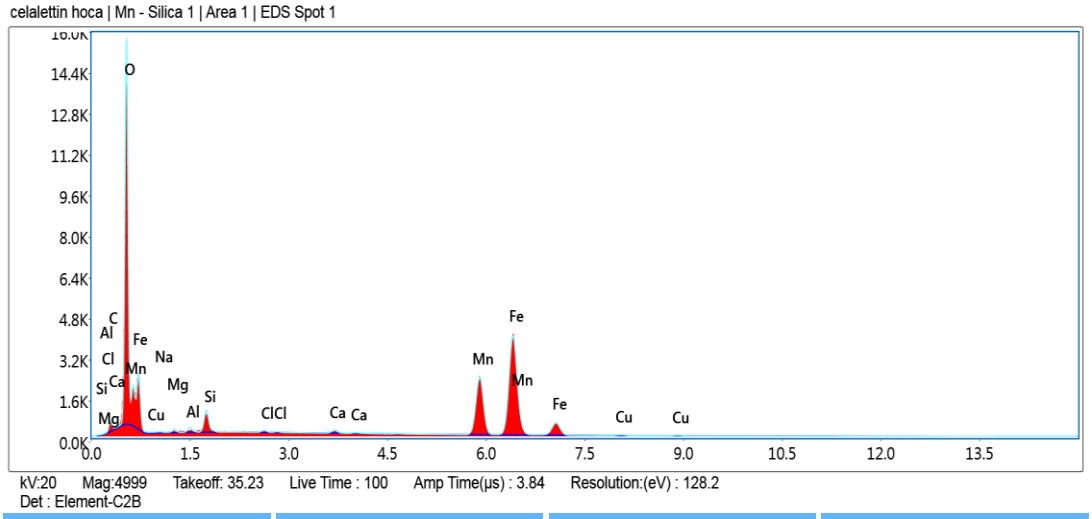

Element	Weight %	Atomic %	Error %
C K	2.60	6.10	13.40
O K	35.00	60.80	6.20
Na K	0.10	0.10	100.00
Mg K	0.50	0.50	22.80
Al K	0.50	0.60	15.70
Si K	2.20	2.20	7.50
Cl K	0.20	0.20	30.50
Ca K	0.50	0.30	17.00
Mn K	19.10	9.70	2.40
Fe K	38.70	19.30	2.00
Cu K	0.60	0.20	23.00

Figure B.8 : EDX of Mn_SC

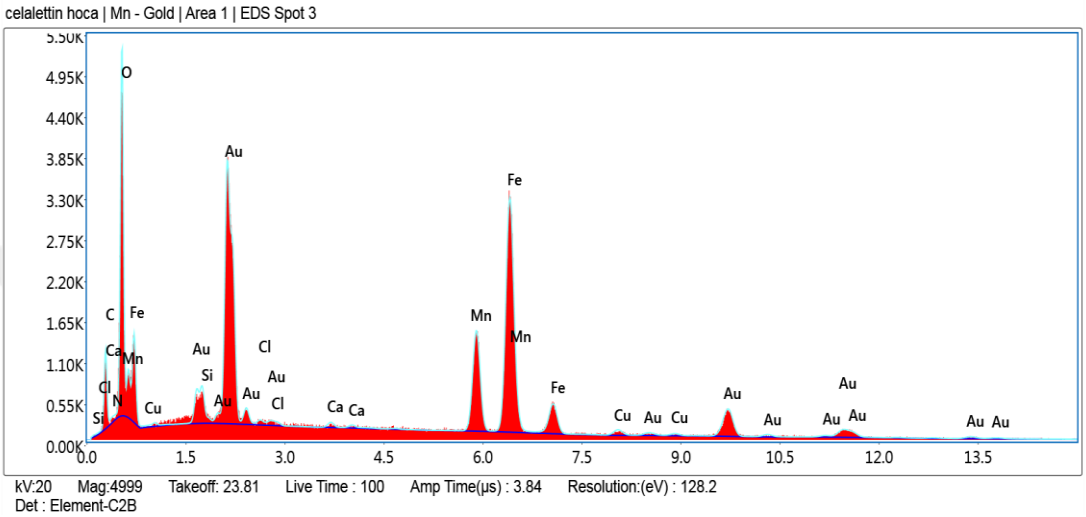

Element	Weight %	Atomic %	Error %
C K	7.00	21.50	10.60
N K	0.00	0.00	100.00
O K	18.80	43.40	8.70
Si K	1.10	1.40	8.90
Cl K	0.10	0.10	73.50
Ca K	0.30	0.30	35.20
Mn K	10.80	7.30	3.60
Fe K	29.30	19.40	2.70
Cu K	1.00	0.60	23.20
Au L	31.60	5.90	10.60

Figure B.9 : EDX of Mn_GASC

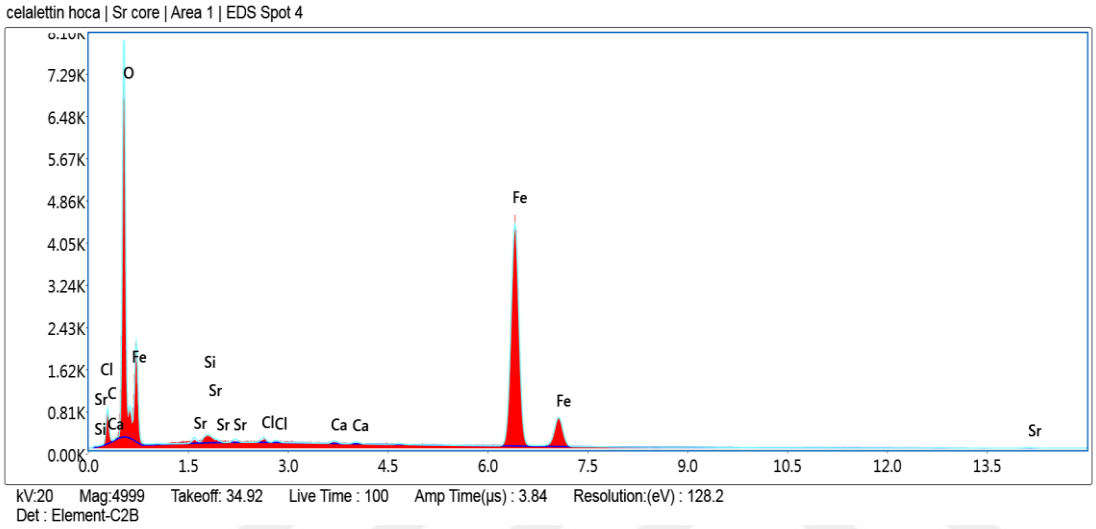

Element	Weight %	Atomic %	Error %
C K	6.90	16.10	10.90
O K	29.70	51.90	7.10
Si K	0.40	0.40	15.00
Sr L	1.00	0.30	11.70
Cl K	0.40	0.30	19.40
Ca K	0.30	0.20	27.10
Fe K	61.40	30.70	1.90

Figure B.10 : EDX of Sr_C

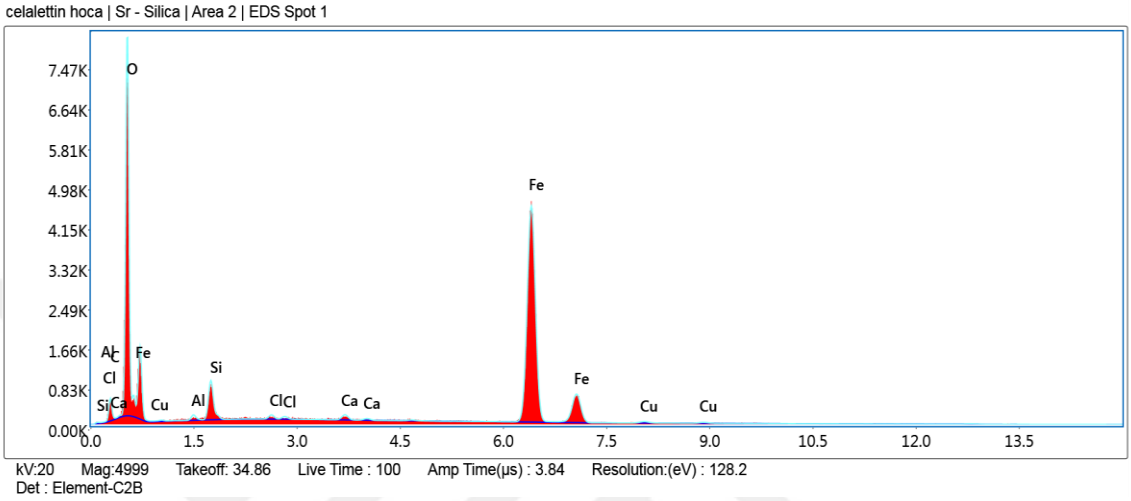

Element	Weight %	Atomic %	Error %
C K	4.60	11.20	12.30
O K	28.60	52.00	7.00
Al K	0.50	0.50	16.70
Si K	2.90	3.00	7.40
Cl K	0.30	0.30	16.70
Ca K	0.60	0.40	14.50
Fe K	61.70	32.10	1.90
Cu K	0.70	0.30	29.60

Figure B.11 : EDX of Sr _SC

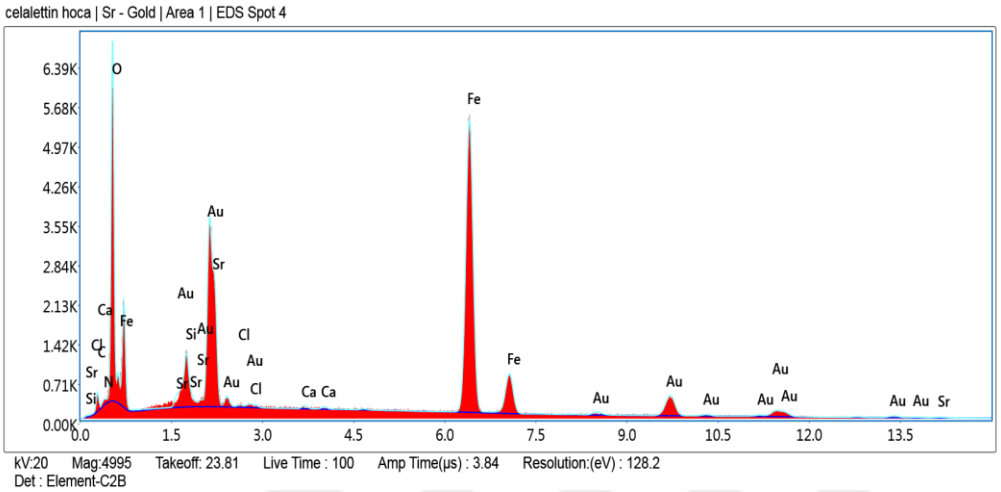

Element	Weight %	Atomic %	Error %
C K	2.10	7.00	14.40
N K	0.20	0.50	87.70
O K	20.60	51.20	8.30
Si K	2.00	2.80	7.70
Sr L	0.80	0.40	9.90
Cl K	0.10	0.10	77.90
Ca K	0.20	0.20	40.50
Fe K	45.10	32.00	2.40
Au L	28.90	5.80	9.90

Figure B.12 : EDX of Sr_GASC

CURRICULUM VITAE

Name Surname **:** Ayşesimay Çetin

EDUCATION:

- **B.Sc.** **:** 2017, Ankara University, Faculty of engineering, Department of Food Engineering

PROJECTS:

- 2018 June-2019 January as a scholar for TUBITAK 1001 PROJECT (project no:214M132, 'Smart nanoparticles for medical application') in İstanbul Technical University, Smart Nanoparticles Laboratuvary.
- 2020 March-2020 July as a scholar for Smart Window Project in Institute for Energy Technology (IFE) in Norway. Production of Hybride Material between Yttrium Hydride Nanoparticles and PMMA for use in Smart Window Project. Production of Hybride Material between Yttrium Hydride Nanoparticles and PEDOT:PSS for use in Smart Window Project.